Student thesis series INES nr 747

Monitoring permafrost degradation in northern Sweden using InSAR technique

Allison Moore

2026
Department of
Physical Geography and Ecosystem Science
Lund University
Sölvegatan 12
S-223 62 Lund
Sweden

Allison Moore (2026).

Monitoring permafrost degradation in northern Sweden using InSAR technique

Master degree thesis, 30 credits in *GIS and Remote Sensing*
Department of Physical Geography and Ecosystem Science, Lund University

Level: Master of Science (MSc)

Course duration: *January* 2025 until *June* 2025

Monitoring permafrost degradation in northern Sweden using InSAR technique

---

Allison Moore

Master thesis, 30 credits, in *GIS and Remote Sensing**

Supervisor:
Zheng Duan
Department of Physical Geography and Ecosystem Science

Exam committee:
Andreas Persson
Department of Physical Geography and Ecosystem Science

Margot Knapen
Department of Physical Geography and Ecosystem Science

Acknowledgements

Thank you to my supervisor Zheng Duan and opponent Chrissi Albus for their invaluable feedback and guidance during this process. Additionally thank you to Margareta Johansson of the Swedish Polar Research Secretariat for providing historic data from the sampling locations.

I am most grateful to have such a supportive community – no one achieves anything alone.

To my parents, Pam and Ken, whose strength and support is unmatched.

To my sister, Hillary, for your unwavering belief in me.

To my brothers, Ben and Harry, for being quiet strength in my corner.

To Juliana and Kanika, for being better friends than anyone deserves and always letting me bend an ear.

And to my wonderful husband Aidan, for everything.

ABSTRACT

Arctic permafrost plays an important role in global carbon storage and has been thawing due to rising temperatures imparted by climate change. Monitoring the active layer thickness (ALT), the seasonally thawing and refreezing uppermost permafrost layer, is essential for understanding permafrost dynamics and their response to warming temperatures. Traditional ALT monitoring relies on ground-based measurements from networks like the Circumpolar Active Layer Monitoring (CALM) program, which provides valuable permafrost data but suffers from limited spatial coverage. To address this, spaceborne Interferometric Synthetic Aperture Radar (InSAR) has emerged as a promising tool and demonstrated feasibility for large-scale ALT estimation, particularly in homogenous permafrost zones (> 50%) of North America. This study evaluated the performance of using InSAR to estimate ALT near Lake Torneträsk in Abisko, Sweden, a sporadic permafrost zone where permafrost coverage is spatially heterogeneous (< 50%). The study area is approximately 2750 km^2 and includes CALM site S2, which contains six sample locations for in-situ validation data. Each of the sample locations covers an area of approximately 100 x 100 m. Synthetic Aperture Rader (SAR) images from Sentinel-1 and soil measurement data taken from Stordalen mire, an area in the study region, were used to produce InSAR-derived ALT estimates. These estimates were evaluated against ground truth ALT measurements for 2018 – 2023.

Overall, the InSAR technique was able to estimate ALT values in the Abisko region, with results showing that ALT has been increasing from 2018 to 2023. Results showed an absolute bias of 0.10–0.40 m and a root mean squared error (RMSE) below the European Space Agency (ESA) Permafrost_CCI threshold of 0.25 m for four out of six of the sample locations. However, the results were only able to be validated for areas close to Lake Torneträsk, due to the limited distribution of the sample locations. The InSAR technique was able to closely estimate ALT in areas with similar soil characteristics as the sample locations, such as the wetland subsets of the study area, but the current model lacks the complexity to generate accurate estimates for different terrains. Future research should focus on expanding the model, allowing for its usage in areas with variable soil characteristics and topography. Assessments of InSAR-derived ALT estimates would benefit from being validated on areas with both a large amount of in-situ measurement data and variation in terrain, vegetation, and permafrost landcover types. This study also compared InSAR-derived ALT estimates to the recently released ESA product, Permafrost_CCI. This product estimates ALT at a resolution of 1 x 1 km using a model based on altitude, temperature, snow depth, and other climate drivers. The comparison revealed that these two estimation techniques largely follow the same pattern, especially in areas with wetland land cover, as is the case with Stordalen mire and the sample sites. The InSAR-derived estimates showed greater deviations in locations outside of the peat wetland areas, such as the mountains in the south of the study area, likely due to the soil characteristics used in model equations not accurately representing the diverging regions.

Contents

1. Introduction

Permafrost, defined as ground that remains at or below 0° C for at least two consecutive years (Harris et al., 1988), has been thawing at increasingly high rates due to climate change. Permafrost underlays around 15% of land in the Northern Hemisphere (Obu, 2021) and is an important geological feature, as it acts as a large carbon store, estimated to hold approximately 1035 ± 150 Pg C (petagrams of carbon) (Mishra et al., 2021). As thaw occurs, mobility and mineralization of organic matter increases causing carbon to release into the atmosphere, which increases the carbon feedback cycle (Stimmler et al., 2023). In addition to greenhouse gas increase, permafrost degradation affects landscape hydrology, soil microbe biology, and geomorphological processes (Åkerman & Johansson, 2008; Johansson et al., 2011), which in turn affect infrastructure stability, plant phenology, and quality of life for people and animals in northern climates. Due to these factors, the field has become an important research topic.

A key indicator of permafrost degradation is the active layer thickness (ALT), which refers to the top layer of permafrost that is subject to annual thawing and freezing (Harris et al., 1988). In Abisko, located in sub-arctic northern Sweden, ALT has been monitored by the Circumpolar Active Layer Monitoring (CALM) program with support from the Abisko Scientific Research Station (ANS) since 1978. The CALM program currently measures six sample sites in the valley located south of Lake Torneträsk which are collectively known as site S2. The sample locations consist mainly of peat plateaus, collapsed palsa, and wet fen (Stiegler et al., 2016). Measurements are gathered during the period of maximum thaw and reported annually. The period of maximum thaw varies for different permafrost locations globally due to microclimates, vegetation, and latitude. For the Abisko region and CALM site S2, maximum thaw occurs in mid to late September, during the second or third week (Strand et al., 2020). The active layers in this sub-arctic region have been observed by CALM to increase by about 0.7 - 1.3 cm per year (Åkerman & Johansson, 2008). The permafrost region in Abisko is classified in many studies as discontinuous and sporadic, while updated modeling classified the region as sporadic and isolated patches, indicating even less permafrost in the area (Johansson et al., 2011; Obu et al., 2019). Permafrost degradation is more rapid in areas where the mean annual air temperature is close to 0°C, such as Abisko (Åkerman & Johansson, 2008). Significant changes in the landscape's permafrost coupled with the difficulty and expense associated with in-person measurements for a vast area make remotely captured data well suited for ALT monitoring. Additionally, ground measurements for active layer thickness are scarce, which hinders the analysis and understanding of permafrost changes, thus amplifying the importance of a repeatable practice that allows for accurate measurements on a large scale. Two

methods used to address this problem are satellite remote sensing and model-based estimations. A proven method for estimating ALT with remote sensing is by using SAR imagery (Liu et al., 2012; Sadeghi Chorsi et al., 2024).

SAR is an active remote sensing technique widely used to capture information about the Earth's surface. SAR utilizes emitted microwaves to generate imagery by measuring the time it takes for the waves to return (Meng et al., 2024). SAR is effective for studying changes in ground objects due to its potential to produce high spatial resolution results, as well as its ability to penetrate deterrent weather, such as clouds, enabling it to be used in any weather or time of day (Zhang et al., 2021). Interferometric Synthetic Aperture Radar (InSAR) is a method of combining two SAR images from separate passes of an area to produce a more refined and precise product. The ESA satellites Sentinel-1A and Sentinel-1B, launched in 2014 and 2016 respectively, capture SAR data, and have a mode of capture called Interferometric Wide (IW) specifically used for building interferograms (Copernicus Program, n.d.). IW has a spatial resolution of 5 m x 20 m and covers a swath of 250 km. Only Sentinel-1A is still active, as Sentinel-1B ceased operations in 2021. With both satellites in operation, the temporal resolution was 6 days. As of 2021, the temporal resolution for captures is 12 days due to only one satellite being operational (Copernicus Program, n.d.).

Remote sensing and InSAR based analysis offer a proven approach to ALT estimation, presenting an opportunity for application in the Abisko region. Other studies have been done in northern Sweden and arctic regions focusing on changing hydrology, freeze thaw dynamics, and peatland degradation (Lakshmiprasad et al., 2024; Seemann & Sannel, 2024; Valman et al., 2024). Valman et al. (2024) utilized InSAR derived from Sentinel-1 data to study surface subsidence and palsa degradation caused by permafrost thaw in northern Sweden, north of Lake Torneträsk. Sadeghi Chorsi et al. (2024) performed InSAR ALT estimations derived from Sentinel-1 data in northern Alaska, which closely aligned with the corresponding CALM field measurements in that region. The absolute error of these estimations was consistently less than the uncertainty of the field data in all years of the study but one. The method used by Sadeghi Chorsi et al. (2024) holds great potential to map ALT on a large scale, thus it is interesting to test in other regions, especially those with scarce in-situ measurements, such as Abisko.

An alternative technique to InSAR based estimations to study ALT is model-based products. A new product released by the European Space Agency in 2024 called Permafrost_CCI uses a permafrost thermal model from the University of Oslo to estimate ALT at a spatial resolution of 1 x 1 km which estimates the annual ALT maximum taken from July – August data. Spanning from 1997 - 2021, this product

covers the arctic area and high mountainous regions in the Northern Hemisphere. Permafrost_CCI is dependent on Landcover CCI, Snow Water Equivalency, and surface temperature data from MODIS and ERA5. The model uses ground temperature and snow levels to model heat latency throughout the thaw season. Due to its recent release, this product has not yet been widely validated or compared to independent InSAR-based estimates. This study will use an established method used by Sadeghi Chorsi et al. (2024) and Liu et al. (2012) that accurately estimates ALT in North American continuous permafrost zones and identify if it is applicable in the study area of the Abisko region which is a sporadic permafrost zone.

Therefore, this study aims to address these knowledge gaps by evaluating the performance of using InSAR technique for ALT estimation in the Abisko region and comparing these estimates with both ground truth measurements and the ESA Permafrost_CCI product. Specifically, this study has three objectives:

(1) Estimate ALT in the Abisko region using InSAR techniques applied to SAR images from Sentinel-1
(2) Evaluate InSAR-derived ALT estimates against in-situ ALT measurements at CALM site S2 within the study area (Abisko region)
(3) Compare in-situ and InSAR-derived ALT estimates with the ESA Permafrost_CCI ALT product to evaluate consistency and identify spatial discrepancies

The research questions addressed with this study are:

(1) How accurately can the InSAR technique estimate ALT in the Abisko region as compared to the in-situ measurements? Accuracy will be determined by using multiple evaluation metrics.
(2) How do the InSAR-derived ALT estimates compare with the ALT estimates from the ESA Permafrost_CCI product in the Abisko region? Patterns of both estimations will be mapped and differences will be analyzed with statistical metrics.

2. Background

2.1 Permafrost Characteristics

Permafrost occurs in high latitudes, such as the north and south polar regions, as well as high altitude locations, such as the Tibetan plateau, which consistently have cold air temperatures. In recent years there has been a push to study the thaw dynamics of permafrost, as the increased thaw threatens the release of large carbon stores (Mishra et al., 2021). Along with the increased activity in the carbon feedback cycle, permafrost thaw and its associated land displacement have the potential to significantly impact infrastructure, such as buildings and railways. Over time, the ground subsidence can

cause changes in the landscape which lead to costly repair work. Therefore, it is important to research how the ground is expected to move and the factors that cause it. Furthermore, the changing landscape affects vegetation health and phenology, as well as the hydrological processes and flow capacity in the region. Permafrost is a complex geological process which differs depending on altitude, soil composition, air temperature, and snow depth, among other factors (Liu et al., 2012). Snow cover has a thermal insulation effect on the ground, but the net effect of increased snow depth in the Arctic is still being investigated (Pedron et al., 2023). Snow is a complex factor of permafrost. While short-term seasonal snow cover lingering into the beginning of summer will insulate permafrost, delaying the thaw onset and reducing ALT at peak thaw time, the year-round snow accumulation can cause insulation of soil from sub-zero temperatures, which in turn causes a net warming and increased thaw (Pedron et al., 2023). How greatly permafrost in a region is affected by snow can change on a yearly basis depending on the depth and accompanying air and ground temperatures of the season. Organic matter and soil moisture impact permafrost by having a cooling effect in the warmer season, insulating effect in the cold season, and in some regions assists in decreasing the active layer thickness by 0.40 m (Du et al., 2023). Given these influences, studying the depth of the active layer is a key indicator of the direction and speed of the thaw. To research permafrost, it is imperative to know which zone occurs in the region being studied, as each has different characteristics.

There are four main classifications of permafrost zones: continuous, discontinuous, sporadic, and isolated patches. Continuous permafrost is defined as underlaying 90-100% of a given area, discontinuous permafrost is defined as underlaying 50-90% of a given area, sporadic permafrost is defined as underlaying 10-50% of a given area, and isolated patches is defined as underlaying less than 10% of a given area. Permafrost transition zones between the classifications are uncertain due to spatial variability. In 1978, the CALM program initiated ALT measurements at site S2 in Abisko, Sweden. At that time, the sample locations within the CALM S2 site included the mountains and the underlying valley and were classified as a discontinuous permafrost zone (CALM). Previous studies done in the area used the discontinuous zone classification while updated permafrost models classify the area as sporadic or isolated patches (Gruber, 2012).

The permafrost modeled by Obu et al. (2019) has a 1 x 1 km spatial resolution and classifies the Abisko study area as mostly isolated patches, with some areas of sporadic and discontinuous zones interspersed closer to the mountains (Figure 1). For the sake of naming in this study, the Abisko region will be referred to as a sporadic zone, as it likely lies between sporadic and isolated patches, depending on the size of land being considered.

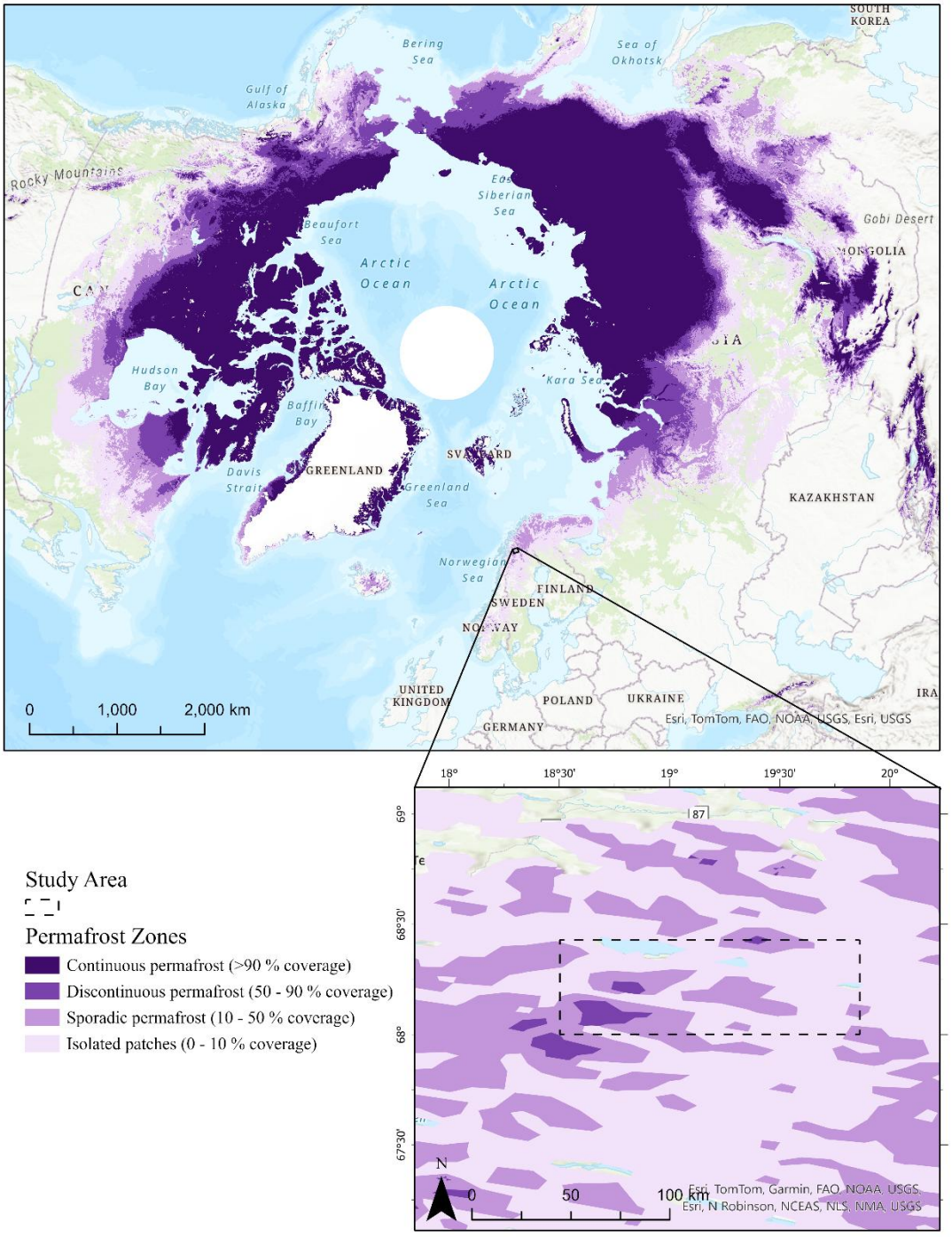

Figure 1: Permafrost zonal map created with data from Obu et al. (2019) study, showing the northern hemisphere in the upper panel and zoomed in to the region of interest for this study in the lower panel.

The active layer of permafrost is the top layer that seasonally thaws and freezes. As the active layer transitions from frozen to unfrozen, it contracts due to liquid water having a higher density than ice. As the active layer refreezes, it expands. This seasonal expansion and contraction cause the upper soil layers to heave up, leading to deformation and subsidence. Several factors affect permafrost thaw and the active layer, such as snow depth, precipitation, air temperature, vegetation, and soil water content. Increased soil moisture increases the soil's thermal conductivity, which results in a thicker active layer (Clayton et al., 2021).

2.2 In-Situ Measurement Methods

There are currently several methods to monitor permafrost activity and active layer thickness. The CALM program uses two in-situ methods to gain ground truth information. The Level 1 method to measure ALT is the mechanical probe method, where a thin, rigid metal rod measuring centimeters is pushed into the soil until it hits firm resistance and cannot be pushed any further (Nelson et al., 1996). This measurement is performed using an established grid system, which involves dividing a 100 x 100 m area into smaller 10 x 10 m zones for sample collection, as outlined by the Active Layer Protocol (Nelson et al., 1996). The Level 2 method involves permanently establishing frost tubes and data loggers in an area, which measure seasonal thaw progression and maximum seasonal thaw. Level 2 measurements are predominantly taken in Northern Canada and Alaska, whereas other field sites primarily use the Level 1 grid probing system.

ALT measurements are available at the CALM database for over 250 sites in the northern and southern hemispheres. CALM data for the northern hemisphere and study area is available here: https://www2.gwu.edu/~calm/data/north.htm. The probed active layer thicknesses reported by CALM can be measured during different times depending on the locations thaw season. In most cases, multiple measurements using the probe method are taken during the thaw season from early June to early September and are averaged to produce a single numeric result (Strand et al., 2020). However, in Abisko, the ALT measurements are sampled using the probe method during the second or third week of September, as this is the time when the maximum thaw is occurring in this area and ALT would be the thickest at this time (Strand et al., 2020). The measurements have historically occurred at 12 sites in the Abisko region, with 9 of the sites being in the valley and 3 of the sites being in the mountainous region. After 2011, only 6 of the valley sites remain as probe locations, with none of the mountain sites reporting numbers. The reason behind the halt in reporting for the mountain sites is unknown, but there is likely still permafrost occurrence as shown by multiple

permafrost probability and extent models in this area (Obu et al., 2019; Westermann et al., 2024a). For this Master thesis, the 6 active sites were used for the 2018-2023 analysis. One site, Torneträsk, stopped reporting measurements after 2021, likely due to having two years in a row with ALT measured at the 1.5 meter mark, which is the upper limit for mechanical probing as stated by the CALM probing guidelines (Nelson et al., 1996). Due to this, only 5 sites were used for the final two years of analysis (2022 and 2023). Additionally, the number of samples taken has decreased, especially at sample locations with thicker ALT measurements, likely due to availability of accessible permafrost via probe. According to Åkerman & Johansson (2008), the number of sampling points at site S2 ranged from 40, 50, 75, and 121, where 121 should be the standard, if possible, to allow capturing of topographic and spatial variability within a sample site (Nelson et al., 1996). During the study years the amount of sampling points has lessened to 30, 45, 70, 77, 82, and 100.

Negative aspects of the in-situ measurements are that the resulting ALT data only covers the immediate area around the measurement, they are labor intensive to secure, and they must be taken every year around the same time to maintain accuracy and provide a trend. Ground truth measurements inherently have uncertainty and variability (Foody, 2024). The accuracy of field measurements can vary for many reasons, including measurement instrument uncertainty, the strength and experience of the probing operator, and the interference of potential buried rock clusters (Strand et al., 2020; Westermann et al., 2024a). Schaefer et al. (2015) found a probing uncertainty of 3 – 8 cm due to thickness of the transition layer at the permafrost table and spatial representation error. The uncertainty attributed to operator strength is cited as not being of significant consideration due to the experience of the operators who gather these measurements and the strict adherence to the CALM sampling protocol (Strand et al., 2020). Furthermore, the potential of buried rock clusters is mitigated by the use of the grid probe system, which helps account for spatial variation in subsurface conditions. It is important to note, however, that a sufficiently large buried rock cluster has the potential to compromise the effectiveness of this mitigation strategy (Strand et al., 2020).

Due to the sparseness of ground measurements globally, it makes interpolation of the measurements difficult. Furthermore, mechanical probing is difficult to accomplish in coarser soils or areas where the active layer is deeper than 1.5 meters (Nelson et al., 1996). Abisko's site S2 average active layer thickness was 0.97 cm as of 2023 (CALM, n.d.), and a few sites in southern Alaska and Canada are close to the 1.5 meter mark (CALM, n.d.). The progressive increase in ALT thickness amplifies the need for a more efficient and widespread measurement system.

2.3 Permafrost Modeling Product – Permafrost_CCI

To quantify how permafrost changes over large areas, new methods must be used. To address this problem, the ESA created a product called the Permafrost_CCI (Climate Change Initiative) using satellite Earth observation methods to provide consistent global mapping of permafrost parameters (Westermann et al., 2024a). The Permafrost_CCI model is based on the CyroGrid2 model from the University of Oslo, which is in turn based on land surface temperature captured from the MODIS satellite, near-surface air temperature data from ERA5, land cover classifications, and other CCI products such as Land Surface Temperature CCI and Snow CCI (Westermann et al., 2024a). The Permafrost_CCI product estimates three variables: ground temperature, permafrost extent, and active layer thickness. The ground temperature product estimates temperature at different depths ranging from 1 – 10 m. The permafrost extent estimates the amount of permafrost within a 1 x 1 km grid cell. The active layer thickness value estimates the annual maximum seasonal thaw depth, which occurs during July – August for most locations. An annual maximum seasonal thaw depth is the maximum temporal resolution possible for this Permafrost Essential Climate Variable (ECV) as designated by the ESA (Westermann et al., 2024b). All variables are provided at a 1 x 1 km resolution. This is the maximum spatial resolution as dictated by the underlying land surface temperature data from MODIS that is used in the CyroGrid2 model (Westermann et al., 2024a).

The coarse spatial resolution of the Permafrost_CCI products are larger than the spatial resolution of both the InSAR estimations, 80 x 80 m, and the ground validation measurements, which cover approximately 100 x 100 m area, the CALM site measurement standard. Permafrost_CCI has been evaluated by the ESA CCI team using pixel-based match-up analysis between estimations and in-situ measurements. For each in-situ location, the pixel in Permafrost_CCI ALT closest to the in-situ site was extracted following the previous studies e.g. Westermann et al. (2024b). This created multiple match-up pairs that were then compared and evaluated. While the spatial mismatch is a known issue and challenge, the match-up analysis of CALM in-situ sites and Permafrost_CCI products provides robust estimations of accuracy and usability of the Permafrost_CCI products (Westermann et al., 2024b). While true for the majority of permafrost areas (continuous and discontinuous) measured by the product, the spatial mismatch is crucial in a sporadic permafrost zone which have large spatial variation within 1 km. The statistical approaches used to characterize errors and uncertainties of the Permafrost_CCI were bias, absolute bias, and root mean square error (RMSE) (Westermann et al., 2024b). To validate the active layer thickness estimates, Permafrost_CCI uses CALM in-situ measurements from all over the northern

hemisphere, except the mountainous regions of Mongolia and Central Asia. All other regions were used for validation, including Abisko and other arctic measurements. Most CALM sites are situated in continuous or discontinuous permafrost zones while only upwards of ten sites are sporadic zones. The majority of Permafrost_CCI ALT estimations validated have between a -0.5 and 0.5 m difference and a median bias of -0.13 m (Westermann et al., 2024a; 2024b). Most of the validation points are located in high latitude continuous permafrost zones, as this is where the majority of in-situ measurements exist. While Abisko was included in the validation, the bias difference is not necessarily representative of the area, as Abisko has sporadic permafrost. It is noted in the Permafrost_CCI validation document that some areas in Scandinavia had up to a -1.5m bias, due to the rocky and pebbled terrain (Westermann et al., 2024b).This calls into question the usability of the Permafrost_CCI results in an area like Abisko.

The Permafrost_CCI product provides an uncertainty value per pixel for each variable listed. Uncertainty is calculated by performing uncertainty propagation though the ground thermal model used as well as adding model uncertainty for neglected processes (Westermann et al., 2024d). The per pixel uncertainty mainly accounts for uncertain landcover and snow cover (Westermann et al., 2024d). In theory the uncertainty could be more robustly evaluated through ensemble methods, but the ESA CCI team found this problematic as many areas with permafrost (high latitudes and high mountain areas) do not have applicable uncertainty of the input data sets (Westermann et al., 2024d). Therefore, the uncertainty pixels provided in the Permafrost_CCI datasets are estimates of parameters that were available (landcover and snowfall), but a comprehensive evaluation is not possible due to the limited validation data available for many of the input parameters.

Active layer thickness is partially dependent on ground stratigraphy, or rock layers (Westermann et al., 2024a). The ground stratigraphy used in the Permafrost_CCI product is the Rock Glacier Inventory (Rouyet et al., 2025). Ground stratigraphy can vary at small distances, leading to inaccuracies when represented by coarser resolutions, as it does not allow for the spatial variability to be represented. This can lead to deviations of several meters in extreme cases and is a known limitation of the Permafrost_CCI product (Westermann et al., 2024a). The WGS84 geographic projection used requires pixel infilling which can smooth out heterogeneous micro-topographies (Westermann et al., 2024b). Furthermore, Permafrost_CCI is stated to have the highest uncertainty within mountainous permafrost areas, such as those in Mongolia and China, as they are more difficult to measure and have less homogenous conditions (Westermann et al., 2024a). The product was released in 2024 but

retroactively creates estimations for 1997 - 2021. However, being a newer product, it has not been widely tested against other InSAR based estimation tools.

2.4 Synthetic Aperture Radar (SAR)

An advantage of using satellite remote sensing to study permafrost is the ability to cover a large amount of area over a long period of time. Permafrost freeze and thaw cycles often cause ground subsidence and heave. To detect these geological changes, a high spatial resolution is necessary to identify small changes over time. The spatial resolution of remotely sensed data is a function of the electromagnetic (EM) wavelength and the length of the satellite antenna, as seen in the following equation (Meyer, 2024):

$$\theta = \lambda \, / \, D \, , \qquad (1)$$

where θ is the beam width (-), λ is the wavelength (m), and D is the antenna length (m). This shows that the beam width, which correlates to the spatial resolution, is a function of wavelength over antenna length. A smaller beam width results in a smaller area of ground surface covered, which in turn results in a higher resolution end product. From this formula it can be deduced that the longer the antenna, the higher the spatial resolution. However, it would be infeasible to send an incredibly long antenna into orbit. To work around this, a method called synthetic aperture was developed in 1952, which uses the combination of a sequence of acquisitions from a short antenna to reproduce the effects of a long antenna (Meyer, 2024). The use of this method in radar is referred to as synthetic aperture radar (SAR) and is used on several active satellites.

SAR is an active data acquisition technique that logs the return of an emitted electromagnetic wave to measure distance from a satellite to the Earth's surface. SAR can operate at different wavelengths of the EM spectrum, most typically using either radio waves or microwaves. SAR uses a side-looking imaging geometry to create a two-dimensional reflective map, where bright spots indicate strongly backscattered signals (Meng et al., 2024). As the radar system flies, imagery taken in the along-track (or azimuth) direction perpendicular to the flight path is called the line-of-sight (LOS). The incident angle is the angle between the SAR beam and a line perpendicular to the surface (Meng et al., 2024).

Analysis of SAR imagery has several applications, such as monitoring oil spills, earthquake mapping and response, supporting search and rescue efforts, and monitoring deforestation. Depending on the topic being researched and the overall purpose, different SAR bands can be used. A band is a range of EM frequencies with a typical use case, which is assigned a letter as a name. For instance, SAR X-band operates with microwaves at a high frequency of 8-12 GHz and a short wavelength of 3.8-2.4 cm.

This produces a high spatial resolution product that is utilized in monitoring snow and ice. SAR C-band operates with microwaves at 4-8 GHz and is a commonly used method for mapping change detection, such as permafrost subsidence, seismic shift motion, and volcanic activity. There are additional bands such as P, L, and S that use lower frequency and longer wavelength to penetrate canopies in order to map vegetation and biomass (Meng 2024).

Since SAR uses an active sensor, there is an ability to control the emitted wave's polarization. Polarization refers to the orientation of the electric field of a wave as it travels to and from the sensor. Different polarizations can offer advantages in revealing distinct surface characteristics, allowing SAR imagery to be tailored to the EM band used and situation being investigated. Another advantage to using SAR is that due to its active and synthetic nature, the wavelengths are able to penetrate clouds and other weather related events which would typically render noisy data from a passive sensor. Additionally, SAR can operate at night, allowing for uninterrupted capture time during its orbit. This is useful for the study area at this northern latitude, which has short daylight hours in the winter and long daylight hours in the summer.

The ESA launched the satellite Sentinel-1A in 2014, followed by Sentinel-1B in 2016, both of which are equipped to capture C-band SAR data at a 20 x 5 m resolution. Given the satellites' global capture schedule, they provide data for any time period since 2014 and 2016 respectively. This temporal range allows for a historical look into geological events. Both satellites are sun synchronous, meaning they pass over a given point on Earth at the same time of day each orbit. The Sentinel-1 satellite operates in the SAR C-band at 5.405 GHz, having a wavelength of approximately 5.55cm (Copernicus Program, n.d.). C-band is an ideal choice for analyzing surface subsidence and permafrost degradation, as it can detect small changes in the surface over short periods of time. C-band is not as overly sensitive to small motion as higher frequency X-bands, and is not subject to as much backscatter as shorter frequency bands, such as the L or P bands (Hogenson et al., 2020). SAR C-band provides a good tradeoff between wave penetration, resolution, and backscatter. However, one limitation of C-band is its inability to penetrate thick canopy or heavily vegetated areas (Copernicus Program, n.d.). C-band can penetrate through the tops of a sparse boreal forest, but is not strong enough to penetrate a very dense or layered canopy. This must be taken into account when considering the area in which a SAR-based product or analysis will be deployed. While C-band is generally a good choice for studying permafrost degradation, it may provide inaccurate results when used to analyze permafrost occurring in densely vegetated areas (Sadeghi Chorsi et al., 2024). The study area for this master's thesis is comprised of wetlands, peat plateaus, and rocky terrain, where C-band is expected to

be suitable. Additionally, the presence of seasonal snowfall in the study area influences both the permafrost insulation as well as backscatter response during SAR image acquisition.

Density and type of snowpack, wet or dry, can affect SAR capture. Wet snow occurs when water is more present in the snowpack as compared to dry snow. This is influenced by the amount of precipitation occurring in the winter months, time of year, sunlight hours, as well as surface roughness and topography beneath the snow. C-band has the potential to penetrate a snow depth of up to 20 m of dry snow and up to 10 cm of wet snow (Tsai et al., 2019). Abisko had a maximum of approximately 10 cm of snow depth during the thaw seasons for 2018 – 2023 (ICOS, 2023), and the area has relatively dry snow due to the low amounts of precipitation during winter months due to its position in the rain shadow of the mountains (ICOS, 2020; Johansson et al., 2011). This makes C-band SAR capture well-suited for the area. The Sentinel-1 satellites that produce the C-band SAR imagery have a capture mode called the Single Look Complex (SLC) which maintains phase information of the swaths. This is necessary to enable the creation of interferograms and utilize InSAR analytics.

2.5 Interferometric SAR (InSAR)

Interferometry is a measurement technique that combines electromagnetic waves to measure phase difference. The phase of a wave at a point in time is its position within a full cycle, expressed as an angle. Phase difference is the difference in phase between two waves with the same wavelength, often caused by time delay. Interferometry is used in a variety of fields, such as astrophysics, oceanography, seismology, and volcanology. Recently, a section of the Great Wall of China was inspected using InSAR to monitor deformation caused by rockslides in the area (Xu et al., 2021).

InSAR is an analysis method which utilizes interferometry and SAR data and can obtain up to a millimeter accuracy. InSAR can be used to detect Earth surface deformation and topographic changes through the comparison of two SAR images that cover the same spot on Earth but were acquired from different positions or different dates (Meng et al., 2024). The phase difference map produced by this method is called an interferogram, which is composed of two SAR images referred to as scenes.

Each interferogram has an associated temporal baseline, which is the time difference in days between scene capture, and a spatial baseline, which is the distance in space between the satellites at time of capture. Coherence, which is the value associated with correlation or quality, is an important factor of an interferogram. Coherence ranges from zero to one, with one being a perfect match in correlation while zero is completely

decorrelated (Zebker & Villasenor, 1992). InSAR signals can become incoherent due to thermal or processor noise, large baseline distance, or rotational viewing geometry where the satellites are looking in different directions (Simons & Rosen, 2007). A simple way to improve coherence is to ensure the interferograms have a short baseline when choosing which ones to use for analysis (Simons & Rosen, 2007). This helps in making sure geometric decorrelation is minimized when possible. Heavily vegetated areas can also negatively affect coherence, due to change over time attributed to growth, or seasonal changes.

By carefully selecting interferograms with low temporal and spatial baselines, phase difference measurements can be primarily attributed to vertical ground displacement that has occurred between captures. In the ideal case, where the spatial baseline is zero, topographic relief has no impact on InSAR phase difference. In interferograms that have a low spatial baseline, phase difference due to topographic relief is negligible when compared to phase difference due to vertical displacement (Simons & Rosen, 2007). Additionally, interferograms with relatively low temporal baseline have negligible phase difference due to horizontal displacement, as over short data time intervals, InSAR is not sensitive to long-term tectonic motion (Sadeghi Chorsi et al., 2024). A digital elevation model (DEM) is used in the interferogram creation process to remove any topographic change, leaving the leftover results to be due to surface displacement.

When creating interferograms, different methods can be applied to reduce noise. One filter commonly applied is the Lee filter, which is a sigma filter that can preserve image sharpness and detail while suppressing noise (Meyer, 2024). Another widely used filter is the Goldstein-Werner adaptive phase filter, which improves fringe visibility and helps reduce additional noise if scenes have low coherence (Goldstein & Werner, 1998). Along with vegetation, water can cause issues with interferograms. Water can have a significant impact on the unwrapping of a measured phase, including water incorrectly being part of the phase fringes (Hogenson et al., 2020). Therefore, a water mask can be applied when processing interferograms to assist in decoherence reduction. Figure 2 is an example of a noisy interferogram. The interferogram appears as random colored noise with no clear patterns that can be used to identify surface motion. This noise is caused by a mix of low coherence values between the two SAR frames and a larger spatial baseline of 18 meters.

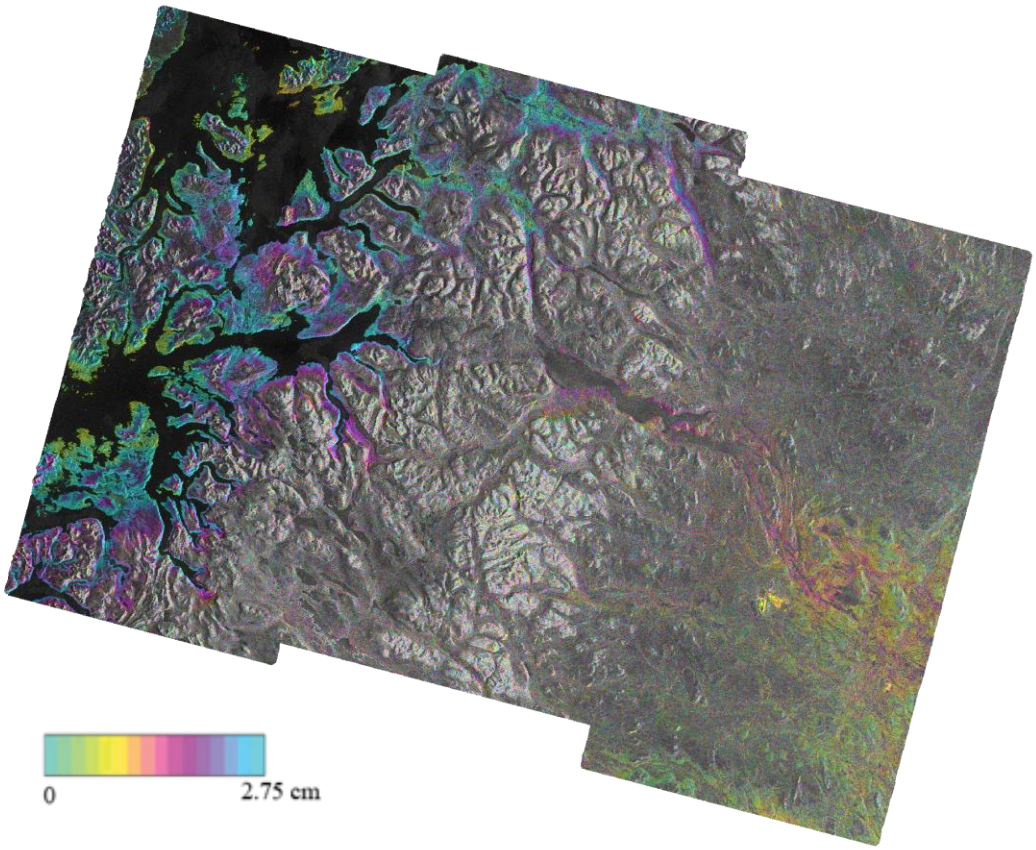

Figure 2 - A noisy interferogram created with SAR images taken April 9th, 2023 and May 3rd, 2023. There is no discernable pattern of color in this interferogram, which does not allow a user to identify phase information relating to surface displacement. In a clean interferogram, each cycle of colors represents the surface movement as phase changes from 0 to 2π, while the noisy interferogram has no discernable pattern.

A clean interferogram has easily distinguishable cycles of color known as 'fringes', which correspond to surface motion. Interferogram interpretation requires knowledge of the EM wavelength used in the input SAR data. The fringes, or changes in each color band, equate to surface displacement of the EM wavelength divided by two (Bamler & Hartl, 1998). For C-band InSAR used in this study, the wavelength is approximately 5.5 cm, making each fringe correspond to a surface displacement of 2.75 cm. The more tightly the fringes are packed together, i.e. many color changes in a short distance on the surface, the more that motion was detected. The wider the fringes are in a given area, the lower the displacement was in that area. An example of fringes and phase cycle is shown in Figure 3 below. The unwrapping of the interferogram starts from the reference point, marked as a white star in the upper right corner of Figure 3. Lines 1 and 2 show surface motion by marking the edge of a phase from 0 to 2π, signified by lines of the same color, in this example purple. Lines 1 and 2 are relatively close together (compared to line 3 on the left-hand side) indicating more surface motion has

occurred between this phase, compared to the phase occurring between line 2 and 3.

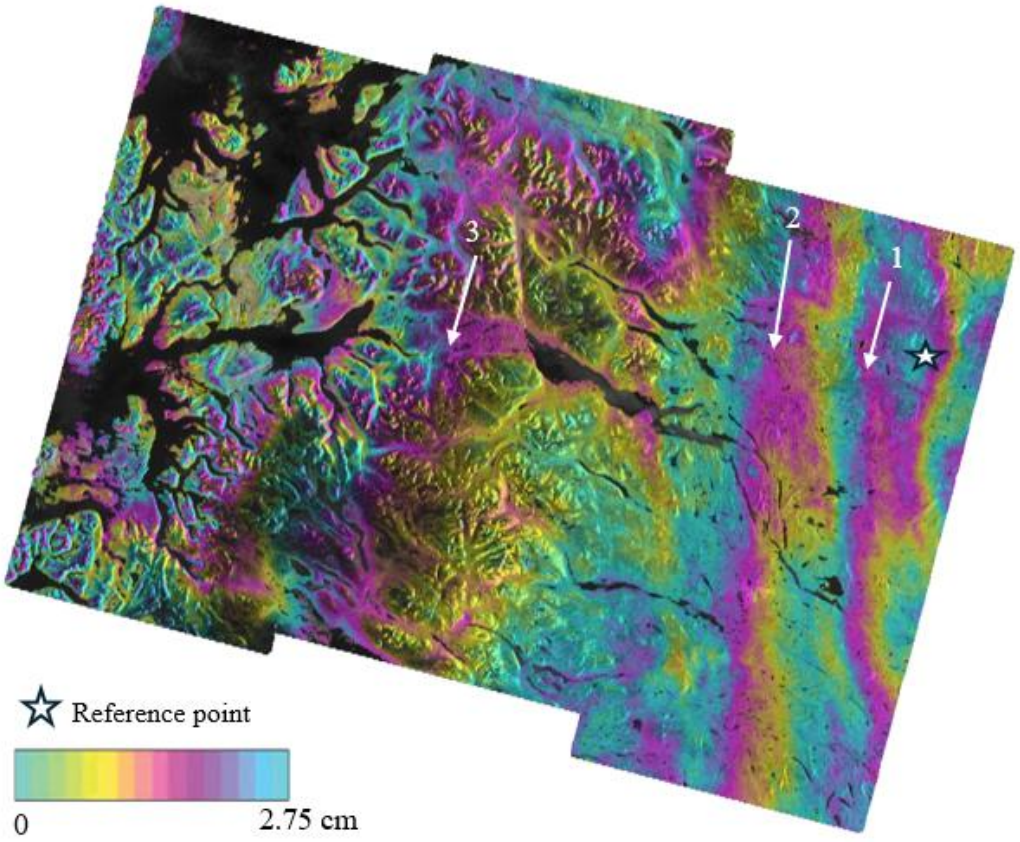

Figure 3 - The interferogram was created using SAR images taken June 13th 2022 and July 31st, 2022, a 48 day temporal difference. This interferogram shows more surface motion on the right side as the cycle of fringes are closer together as indicated by the distance between the arrows. Between the two diagrammed fringes is a phase difference of 2π.

Permafrost and active layer thickness cannot be identified solely with remote sensing techniques. InSAR can measure surface deformation as a proxy for active layer thickness (Sadeghi Chorsi et al., 2024). However, InSAR has limitations such as the reliability of the results given the ground land cover and soil moisture. As InSAR is created through interferometry of SAR images, the limitations of the SAR band used are also applicable, such as the inability to penetrate dense canopies due to wavelength limitations.

2.6 Previous Studies

2.6.1 Remotely Sensed Permafrost Research

Since permafrost itself cannot be easily studied with remote sensing, it is the effects of permafrost, which act as indicators to its health and cycle, that are studied. Active layer thickness and degradation are key permafrost variables and are the focus of many studies using InSAR in a variety of permafrost classifications and locales. Sadeghi Chorsi et al. (2024) and Liu et al. (2012) studies focus on estimating ALT near the

Alaskan North Slope continuous permafrost zone. Chen et al. (2020) study occurred in the same area but focused on the water storage dynamics within the freeze thaw cycle as detected from interferograms. Valman et al. (2024) estimated surface degradation among palsa peatlands in northern Sweden, northeast of Lake Torneträsk and along the Swedish border. Michaelides et al. (2019) investigated post-fire dynamics and effects on vegetation, soil moisture, and active layer thickness using InSAR in southwestern Alaska's discontinuous permafrost zone. These studies helped shape the way permafrost can be investigated and estimated with InSAR techniques, which in turn helped inform the methods of this master's thesis.

One class of permafrost effect which is studied using InSAR is the thermokarst or melted ground ice which takes the shape of ponds on the landscape (Liu et al., 2015). These surface deformations occur due to erosion of the land under massive ground ice as it melts and can occur in a variety of places. Liu et al. (2015) investigated a growing thermokarst between the Trans-Alaska pipeline and the main highway in that region of Alaska, showcasing the importance of monitoring degradation as it can impact infrastructure.

In Barrow, Alaska, research was conducted to estimate ALT using LiDAR and NDVI data (Gangodagamage et al., 2014). LiDAR is a remote sensing technique that uses pulsed lasers to measure distances to objects on the surface and NDVI is a normalized difference vegetation index. Gangodagamage et al. (2014) were able to estimate ALT at a 2 x 2 m resolution with an RMSE of ± 4.4 cm. These remotely sensed results were evaluated against the ground truth data from the CALM site in Barrow, Alaska. The results are fairly accurate, considering the Permafrost_CCI product allows an RMSE range of 25 cm. Additionally, a discovery of the study was that while rising air temperatures are partly responsible for the overall regional thawing trend seen in permafrost, smaller scale variability is largely controlled by local factors such as hydrology and geomorphic composition. Also studied in Barrow, Alaska in 2015 was a product called the Remotely Sensed Active Layer Thickness (ReSALT). Using this method, the ALT was accurately estimated in 76% of the study area within the margin of uncertainty associated with ground penetrating radar and CALM probing measurements (Schaefer et al., 2015). However, this study discovered that about 22% of the product's predictions underestimated ALT, especially in areas with well-draining soils or soil containing gravel.

Alaska has large amounts of continuous and discontinuous permafrost making it an ideal place to study ALT estimations, particularly along the Northern Slope. Liu et al. (2012) performed studies to estimate ALT on the Northern Slope as well as measure

surface deformations. This master's thesis uses a method that was successfully performed by Sadeghi Chorsi et al. (2024) for the Alaskan North Slope.

2.6.2 Permafrost Research in Abisko, Sweden

Åkerman & Johansson performed a study to measure the regression rate for each individual sample location at the Abisko site in 2008. They studied how mean air temperature, snow depth, and precipitation affected the permafrost regression trend from 1978 - 2006. This study also reported the decline in sample points in the gridded sample area. After 1998, there was a steady and steep decline in the number of sample points available for ground measurements in Abisko. All of their measurements rely on in-situ data, which is the basis by which this study was able to validate ALT estimations.

Strand et al. (2020) found that peat thickness, wetness, and microtopography all play a role in the ALT differences found among the sample locations in Abisko. This is important for this Master's thesis as soil porosity and saturation are included in the method calculations for ALT. The values from Stordalen Mire were used as a proxy for the region but knowing that variety in thickness and wetness impacts ALT estimation could potentially account for errors (Clayton et al., 2021).

3. Study Area

Located in northern Sweden, the study area is in the sub-arctic region near Abisko, covering approximately 55 x 50 km, or 2,750 square kilometers. The study area, shown below in Figure 4, is south of Lake Torneträsk and includes Abisko National Park and Stordalen Mire. The Abisko region has an unclear permafrost zonal index, with models considering it either sporadic or isolated patches, which contain a low percentage of permafrost underlaying a given area. The study area includes CALM site S2. Site S2 is comprised of six sample locations as shown below in Figure 4, each measuring approximately 100 x 100 m. Four of the sample locations are on the southwest side of Lake Torneträsk and west of Stordalen Mire, while the other two are of the southeast side, as shown in Figure 4b and Figure 4c. Active layer thickness measurements are taken at each of the six measurement locations and reported in the CALM database. A 55 x 50 km study area around S2 and Lake Torneträsk (black dashed box in Figure 4a) is used for this thesis' study of ALT estimation based on InSAR-derived surface displacements captured throughout the thaw season.

The sample locations are located at elevation 380 – 480 m above sea level. The measured sites are peatlands, with varying depth of 1 – 3 meters. The Storflaket area is a peat plateau and Torneträsk is a collapsed palsa (Stiegler et al., 2016). In the study area, the Stordalen mire is an area consisting of wet fen which has been studied since the 1970s. Due to the extensive research at Stordalen mire, soil measurement data from

this area was available for use in determining soil characteristics. According to the Swedish Meteorological and Hydrological Institute (SMHI), during the years of this study, 2018 – 2023, the average air temperature in Abisko area was 0.9° C. According to Integrated Carbon Observation Surface (ICOS), the average ground temperature during this time frame was -0.78° C.

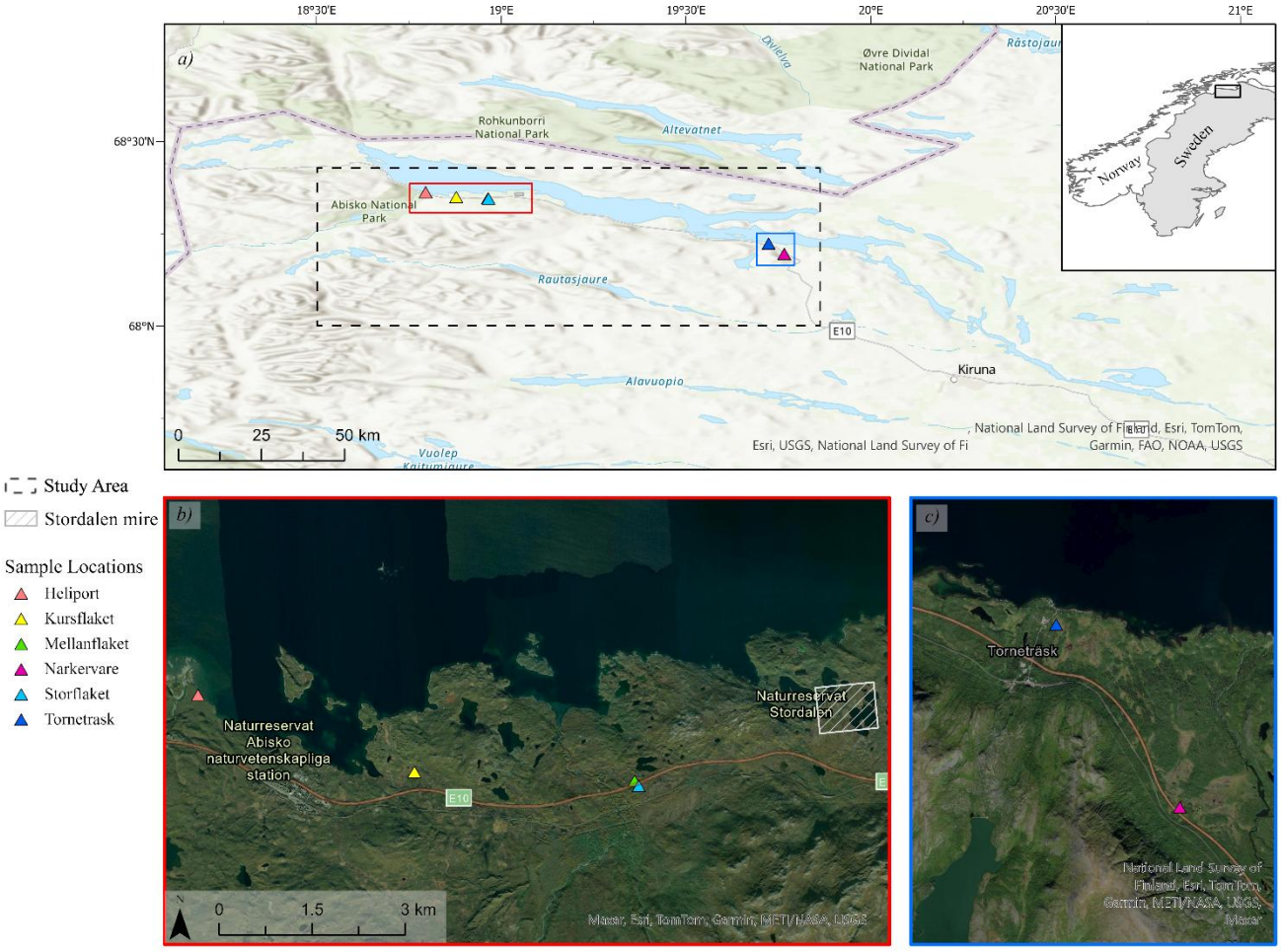

Figure 4: Map A shows the boundary of the study area as well as the six sampling sites used as ground truth. Together these sites make up the CALM site S2 – Abisko, Sweden. Map B are the detailed sites on the west side of Lake Torneträsk along with Stordalen mire, where the soil characteristics data was taken, while Map C shows the two sample sites on the east side of the lake.

This region was chosen for this thesis due to the changing permafrost dynamics in the area. Additionally, the area was chosen because it is manually probed yearly which provides validation data. Ground truth measurements in Scandinavia are scarce due to the limited amount of permafrost left in the region. The availability of the in-situ measurements to be used for validation is a strong reason to study this area. The study area fits entirely within a single SAR image, which avoids the potential for errors

associated with mosaicking multiple SAR images together, such as geometric misalignment.

4. Data

4.1 Remotely Sensed Data

To perform this analysis, SAR data was acquired from Sentinel-1A and Sentinel-1B C-band over the study area in northern Sweden, utilizing tracks 95 and 168. The SAR images used are Single Look Complex (SLC), which maintains phase information, making it useful for creating interferograms. The data was captured using Interferometric Wide swath mode (IW) with a dual polarization of VV + VH. Additional details regarding the sensor onboard Sentinel-1A and Sentinel-1B can be found in Section 2.4. The data has a spatial resolution of 5 m x 20 m and covers a swath of 250 km, with a temporal resolution of 12 days for one Sentinel satellite pass. Both Sentinel-1A and Sentinel-1B data were used in this study for years 2018 - 2021, allowing for a 6-day temporal resolution. For years 2022 and 2023, only Sentinel-1A data was used due to data availability, resulting in a 12-day temporal resolution.

The SAR images were used to create interferograms which show surface subsidence and motion between the two capture dates. For example, if SAR image one was taken April 1 and SAR image two was taken April 15, the interferogram created from these would show the ground motion between these dates. The thaw season start and end dates were used as guidelines to search for SAR images, as this is the time of year needed to capture surface subsidence to calculate ALT. It is important to use multiple interferograms from throughout the thaw season with shorter temporal baselines (a smaller number of days in between the two SAR images used) so the motion is attributed to ALT instead of outside factors, such as vegetation or phenology changes of the season (Simons & Rosen, 2007).

The output calculated using all the interferograms for a given year results in the maximum ALT for that year. The maximum ALT estimated from calculations of the interferograms was then comparable to the in-situ data, which is also reported annually (CALM, n.d.). The maximum thaw season depth is equivalent to ALT for the year and annual is the highest temporal resolution possible for ALT as specified by the ESA (Westermann et al., 2024b).

Table 1: Date ranges used for searching for SAR data to create the interferograms. Date ranges are found by utilizing thaw start and end dates and the dates to not exceed. Each years range falls within the thaw start and thaw end dates for the respective year.

Year	Interferogram Start Date	Interferogram End Date	Number of Interferograms Used
2018	April 17	September 14	31
2019	June 5	September 21	17
2020	April 12	October 27	38
2021	May 1	October 16	34
2022	May 8	October 23	9
2023	April 9	October 6	9

The interferograms were created and downloaded from the Alaska Satellite Facility tool Vertex, located here: https://search.asf.alaska.edu. The resulting interferograms have a spatial resolution of 80 x 80 m and a temporal resolution dependent on the two interferogram dates, typically between 12 and 30 days. The interferogram resolution is 80 x 80 m due to a process called multilooking, which explained further in Section 5.1.

Remotely sensed measurements of hourly pressure levels obtained from the Copernicus Climate Change Service, Climate Data Store were used to perform atmospheric corrections using the python package PyAPS by Jolivet et al. (Copernicus Climate Change Service, Climate Data Store, 2023; Jolivet et al., 2011). The PyAPS package by Jolivet et al. can be accessed here: https://github.com/insarlab/PyAPS. This assists in mitigating the tropospheric propagation delay that affects C-band SAR data, which is discussed further in section 5.2.

4.2 In-situ Measurements

Soil temperature data at the Stordalen mire (68°21′20″N, 19°2′47″E) is recorded by the Integrated Carbon Observation Surface (ICOS) on an intraday basis (ICOS Sweden, 2023; Lundin et al., 2025). Stordalen mire is located south of Lake Torneträsk, shown in Figure 4b. The soil temperature information was used as surface temperature readings to calculate thaw season start, thaw season end, and accumulated thaw days. Table 2 notes the thaw start and end date as determined by the surface temperature data. These dates are found by a process Accumulated Degrees Day Thaw (ADDT) described further in Step 1 of Section 5.3. Snow depth data at Stordalen mire is recorded by ICOS and the ground is snow free or has minimal snow (up to 2 - 3 cm) during the thaw season date ranges in Table 2.

Table 2: Date ranges used for thaw season as determined by soil temperature values from Stordalen mire, Abisko, Sweden.

Year	Thaw Start Date	Thaw End Date
2018	May 3	October 27
2019	April 20	October 8
2020	May 12	October 17
2021	May 7	October 17
2022	May 6	November 14
2023	May 6	October 16

Soil porosity and saturation data was accessed from a study published in 2022 by Palmtag et al., via the Bolin Centre Database (Palmtag et al., 2022). This study analyzed soil from 16 sample locations across the northern permafrost region, including Abisko, Sweden, near the Stordalen mire. Only data from Stordalen mire was used in this study as it is representative of soil characteristics near CALM site S2 sample locations. The data is utilized in Step 3 of Section 5.3.

In-situ measurements of the active layer thickness were recorded by CALM for site S2 in Abisko. Site S2 contains six sample sites representing the ALT of the peatlands in the study area. While six sample locations may seem a small number, this is typical for permafrost ALT measurements. Liu et al. (2012) utilized six sample locations, Schaefer et al. (2015) had four validation sites, and Sadeghi Chorsi et al. (2024) had one CALM validation site. In Sadeghi Chorsi et al. (2024), the CALM validation site area covered roughly the same percentage of their total study area as in this master's thesis study. These measurements are taken annually at each site within a 100 x 100 m grid, which is the CALM site standard. Measurements are probed during the maximum thaw period which occurs in the second - third week of September (CALM, n.d.; Strand et al., 2020). For use in this study, all six active sample locations were used for years 2018-2021. For the final two years of the study, 2022 and 2023, Torneträsk (Site AB4) did not report measurements, reducing the sample locations available to five. These in-situ measurements are used as ground truth data to determine the accuracy of the InSAR estimated measurement.. These six sites are chosen as they offer essential ALT validation data. Additionally, their composition of sporadic permafrost within peat wetlands intermixed with other vegetation is representation of the broader area's composition.

The measurement locations shown in Figure 4 are listed below in Table 3 citing location, elevation, and other relevant data, gathered from the CALM Abisko metadata and the Åkerman & Johansson study in 2008 (Åkerman & Johansson, 2008; CALM, n.d.). CALM measurements can be accessed through this site: https://www2.gwu.edu/~calm/data/north.htm.

Table 3: Individual measurement sites within CALM S2 and the corresponding site codes, elevation, and number of sample points. The number of sample points is taken from Åkerman & Johansson (2008).

Site Code	Site Name	Coordinates	Elevation (m)	Number of Sample Points
AB 5	Heliport	18°47'44"E, 68°21'52″N	385	121
AB 2	Kursflaket	18°52′42"E, 68°21'05"N	391	55
AB 3	Mellanflaket	18°57′51"E, 68°20′53″N	390	40
AB 1	Storflaket	18°57'55"E, 68°20′51"N	380	121
AB 4*	Torneträsk	19°43′24"E, 68°13'32"N	390	40
AB 11	Narkervare	19°45'57"E, 68°11'52"N	480	75

* For site AB4 - Torneträsk, active layer thickness ground measurements are only available for the 2018-2021 years of this study. There is no data for the final two years investigated, 2022 and 2023.

4.3 ESA Permafrost_CCI

The ESA created a permafrost product, Permafrost_CCI, which includes ALT estimations, ground temperature interpolations, and permafrost extent for the Northern Hemisphere for 1997 – 2001. For this study, the ALT estimations were utilized to compare against the InSAR derived estimations and the ground truth data. The Permafrost_CCI product has a spatial resolution of 1 x 1 km and a produces the maximum value estimated for the thaw season, around July - August. This is the listed temporal resolution for this product as many permafrost locations in the Northern Hemisphere have maximum thaw within this time frame (Strand et al., 2020; Westermann et al., 2024c). The maximum thaw is measured in late summer and is representative of ALT for the specified year (Westermann et al., 2024b). According to the ESA, users of this product have expressed interest in higher temporal resolution then the annual number, however an annual resolution is the highest temporal resolution possible for this product (Westermann et al., 2024b). While it is technically possible to obtain the seasonal thaw depth evolution through estimations, this is not an Essential Climate Variable (ECV) deemed by the ESA (Westermann et al., 2024b). To measure ALT the highest temporal resolution is once a year. The Permafrost_CCI product has a coarser resolution compared to the ground truth measurements and the interferograms that estimate ALT, which are 100 x 100 m and 80 x 80 m, respectively. Additional details regarding the Permafrost_CCI product can be found in Section 2.2. The ESA Permafrost_CCI active layer thickness, extent, and ground temperature data is available here for the study years:

https://catalogue.ceda.ac.uk/uuid/d34330ce3f604e368c06d76de1987ce5/

https://apgc.awi.de/dataset/permafrost-cci-alt-north-hemisphere-v4-1997-2021

5. Methodology

To estimate the yearly active layer thickness, interferograms were created from SAR data from 2018 – 2023 following the methodology used in Sadeghi Chorsi et al. (2024). The interferograms line of sight values represent surface motion. An atmospheric correction was performed on each interferogram to adjust for particles in the troposphere that can cause noise in the signal (Liu et al., 2012; Sadeghi Chorsi et al., 2024). ALT was estimated by first calculating accumulated degree days of thaw, seasonal vertical surface displacement amplitude, and soil parameters. These values were then used in the ALT estimation calculation. These InSAR derived ALT estimations were extracted at ground truth measurement locations within the study area for comparison. An 80 x 80 m grid of values covering the entire study area was also extracted and resampled to compare against the Permafrost_CCI ALT estimation product. These methods are described in detail below.

5.1 Interferograms

To measure the active layer thickness, SAR data was utilized from paths 95 and 168 to create interferograms of the study area during the 2018-2023 time period. Each interferogram uses two satellite images called scenes or granules. The interferograms produced will show ground displacement in the area via the phases of the radar imagery, which are converted to line of sight (LOS) displacement values later used to estimate ALT. For this study, between 9 and 38 interferograms were created for each year from 2018 to 2023 across the thaw season, approximately mid-April to October, depending on the year (see Table 1). The method for finding the thaw season start and end is outlined in Step 1 of Section 5.3.

Interferograms were created using the Vertex tool from the Alaska Satellite Facility (ASF). SAR scenes have a spatial resolution of 5 x 20 m. The output interferogram has a resolution of 80 x 80 m due to a process called multilooking. Multilooking takes a number of passes or “looks” in the azimuth direction, along the satellite path, as well as a number of looks perpendicular to the satellite’s path (Alaska Site Facility, n.d.; Zebker & Villasenor, 1992). The number of looks, in this instance 20 x 4, is multiplied by the spatial resolution, 5 x 20 m. This results in a 100 x 80 m interferogram that is then resampled to 80 x 80 m. Scenes with a small spatial baseline were chosen, as these have the highest coherence, which is an important factor in producing an accurate interferogram. When processing the interferograms, a water mask was applied to remove water bodies from the scenes, as water can affect the coherence values and lead to decorrelation (Hogenson et al., 2020). The water mask is created by ASF using data from OpenStreetMap to identify coastal waters and inland water bodies. Smaller inland

water bodies are not considered to be water by the mask (Hogenson et al., 2020). Not every interferogram's water mask worked successfully, as when individual interferograms were inspected, a few still had water in the Torneträsk lake area. However, for these scenes, the coherence values were inspected on a case-by-case basis. After evaluation, the coherence values were in line with those values in scenes where the water mask completely removed all of the lake water. Therefore, both scenes with and without a complete water mask were used, as long as the coherence values were not compromised. The ASF Vertex tool has a built-in noise filtering feature, the Goldstein-Werner adaptive phase filter, which is able to improve coherency, which in turn improves fringe visibility and allows for more accurate interferograms (ASF Metadata, Goldstein & Werner, 1998). This filter has a default of 0.6 and can be increased manually (up to maximum 1) if coherence levels look particularly low. The digital elevation model Copernicus DEM GLO-30 dataset was used as a base for geoid corrections.

After the filtering and water masks were applied, phase unwrapping was performed within ASF's Vertex tool. For this, a reference point was selected, which is typically a point with high coherence in a stable (not noisy or fuzzy) local region . The Vertex tool was used with a rolling maximum search window of 9 x 9 pixels to identify the region with maximum coherence. The reference point was chosen from this region, and the unwrapping phase began relative to this point. From here, the interferograms were processed and geocoded. The output consisted of several geotiff files, including a line of sight displacement map, incident angle map, amplitude, coherence, and look vectors.

5.2 Atmospheric Correction

The interferograms were then corrected for atmospheric delay. A leading cause of errors in InSAR processing is attributed to atmospheric effects (Meyer et al., 2006). The troposphere is the layer of atmosphere closest to Earth, and the tropospheric impacts can heavily affect C-band SAR data (Meyer, 2011), causing noise and decoherence.

The basis for modeling the atmospheric phase delay is the line of sight (LOS) single path tropospheric delay, calculated as the integral of air refractivity between surface elevation z and the elevation of the reference point, z_{ref}, as shown in the following equation (Jolivet et al., 2011):

$$\delta L^{s}_{LOS}(z) = \frac{10^{-6}}{cos(\theta)} \left\{ \begin{array}{c} \frac{k_1 R_d}{g_m} \left(P(z) - P\left(z_{ref}\right) \right) \\ + \int_{z}^{z_{ref}} \left(\left(k_2 - \frac{R_d}{R_v} k_1 \right) \frac{e}{T} + k_3 \frac{e}{T^2} \right) dz \end{array} \right\}, \qquad (2)$$

where $\delta L^{s}_{LOS}(z)$ is the LOS single path tropospheric delay at surface elevation z (m). The first term in the sum addresses the dry air component of the delay path and the second term addresses the air moisture. θ is the incidence angle (°), $R_d = 287.05\, J \cdot kg^{-1} \cdot K^{-1}$ represents the dry air constant, and $R_v = 461.495\, J \cdot kg^{-1} \cdot K^{-1}$ represents the water vapor specific gas constant. g_m is the average gravitational acceleration between z and z_{ref} $(\frac{m}{s^2})$. The 2014 improvement of this model by the same author sets $g_m = 9.8 \frac{m}{s^2}$ (Jovlivet et al, 2014). P is the dry air partial pressure (Pa), e is the water vapor partial pressure (Pa), and T is the temperature (K). The constants are $k_1 = 0.776\, K \cdot Pa^{-1}$, $k_2 = 0.716\, K \cdot Pa^{-1}$, and $k_3 = 3.75 \times 10^3\, K \cdot Pa^{-1}$ (Smith and Weintraub, 1953). z_{ref} is the elevation at which the atmospheric delay is nearly constant with respect to time. z_{ref} is typically chosen to be $10{,}000\, m$.

To run this equation, a Python package called PyAPS3 was used, created by Jolivet et al. (2011). To identify the tropospheric phase delay, information about the water vapor and air pressure was needed. These values were provided by the Copernicus Climate Change Service, Climate Data Store, where they were queried for the day and hour that the individual SAR scenes that produce the interferograms were taken. Additionally, the incidence angles and line of sight displacements were taken from the outputs of ASF's Vertex tool, which was used to create the interferograms. Elevation values were also needed, which are provided by the digital elevation model (DEM) used to create the interferograms. The tropospheric delay was calculated for both scenes that went into the interferogram. The delay arrays were subtracted from each other, giving a total delay for the interferogram. The total delay array was then subtracted from the line-of-sight values, leaving the new line of sight values atmospherically corrected.

5.3 Active Layer Thickness Estimation

The active layer thickness was estimated using the method presented in the Sadeghi Chorsi et al. (2024) study for years 2018 – 2023 in the study area. The Python code for implementing the method is available here: https://zenodo.org/records/10023340. This code was modified for the purposes of this Master's thesis to utilize variables adjusted for the study area, such as local soil porosity, thaw dates, etc. In brief, ground temperature data, soil measurement values from Stordalen mire, and the atmospherically corrected interferograms were processed to create the active layer thickness estimations, as outline in Figure 5. The details of each step are described below in the subsections. The displacement values outputted by the code were attributed to vertical ground motion, justified by the selection of interferograms with low spatial and temporal baselines, as discussed in Section 2.5.

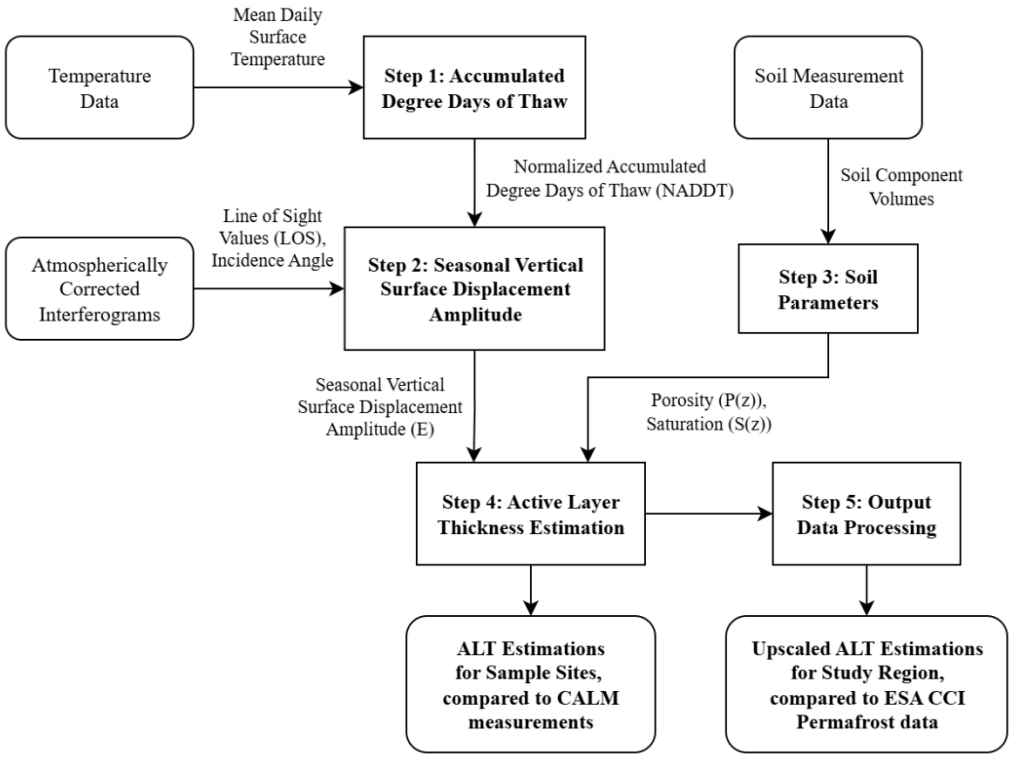

Figure 5: A flowchart showing the five steps for estimating active layer thickness using the modified Python code, as described in Section 5.3. Input data sources and output data are shown for each step.

Step 1: Accumulated Degree Days of Thaw

First, daily ground temperature data for a given year was used to calculate the accumulated degree days of thaw (ADDT). ADDT represents the total thaw that has occurred by a date in the thaw season, and is defined and estimated by the following equation (Riseborough, 2003):

$$ADDT = \int_0^d (T_s - T_f)dt \approx \sum_{i=0}^{d} \overline{T}_{s,i}\,, \qquad (3)$$

where d is the number of days since the start of the thaw season, T_s is the surface temperature ($°C$), T_f is the freezing point of water ($0°C$), $\overline{T}_{s,i}$ is the mean surface temperature on day i ($°C$), and ADDT is expressed in $°C \cdot days$. Daily average surface temperature data gathered from Stordalen mire (ICOS) was used for $\overline{T}_{s,i}$. Only days with positive mean surface temperature were used in ADDT calculation. For each year, the thaw season start was found by locating the first day with positive mean surface temperature where, when calculating ADDT from that day onwards, a threshold value of 10 $°C \cdot days$ is reached before a negative mean surface temperature is encountered. Similarly, the thaw season end was found by finding the day before the first day with

negative mean surface temperature where, when calculating ADDT (considering only negative mean values) from that day onwards, a threshold value of -10 $°C \cdot days$ is reached before a positive mean surface temperature is encountered.

ADDT was calculated for both the entire thaw season and for each interferogram's two capture dates. Normalized ADDT was then calculated for each interferogram's two capture dates. Normalized ADDT is a representation of the fraction of total thaw that has occurred by a date in the thaw season, and is defined and estimated by the following equation:

$$NADDT_d = ADDT_d \,/\, ADDT_w \approx \sum_{i=0}^{d} \overline{T}_{s,i} \,/\, \sum_{i=0}^{w} \overline{T}_{s,i}\,, \qquad (4)$$

where d is the number of days since the start of the thaw season and w is the duration of the whole thaw season in days. $NADDT_d$ is the normalized ADDT d days into the thaw season (-), $ADDT_d$ is the ADDT d days into the thaw season ($°C \cdot days$), $ADDT_w$ is the ADDT for the whole thaw season ($°C \cdot days$), and $\overline{T}_{s,i}$ is the daily mean surface temperature ($°C$).

Step 2: Seasonal Vertical Surface Displacement Amplitude

Next, the seasonal vertical surface displacement amplitude, E, was calculated for each chosen point. The line of site (LOS) data provided by the interferogram creation was divided by the cosine of the incidence angle to produce a vertical displacement, D. The relationship between vertical displacement and vertical surface displacement amplitude at a given point is expressed by the following equation (Liu et al., 2012, Schaefer et al., 2015):

$$D_j = \frac{LOS_j}{cos(\theta_j)} = E_j \cdot \left(\sqrt{NADDT_2} - \sqrt{NADDT_1}\right) + \varepsilon\,, \qquad (5)$$

where for point j, D_j is the vertical displacement (m), LOS_j is the line of sight value (m), and θ_j is the incidence angle (°). E_j is the seasonal vertical surface displacement amplitude (m), $NADDT_1$ and $NADDT_2$ are the normalized ADDT values for the two capture dates of the interferogram (-), and ε is an error term for unknown error sources and noise (m). For each year, a linear least squares estimate was performed using data from all interferograms to estimate E_j at each point.

Step 3: Soil Parameters

In addition to surface temperature, two key components of permafrost mechanics are the porosity and saturation of the soil. Porosity and saturation are defined in the following equations (Jasoliya et al., 2024):

$$P = \frac{V_v}{V_T} = \frac{V_w + V_a}{V_T}\,, \qquad (6)$$

$$S = \frac{V_w}{V_v} = \frac{V_w}{V_w + V_a}, \qquad (7)$$

where P is the porosity (-), S is the saturation (-), V_T is the total soil volume ($\frac{kg}{m^3}$), V_v is the volume of voids in the soil ($\frac{kg}{m^3}$), V_w is the volume of water in the soil ($\frac{kg}{m^3}$), and V_a is the volume of air in the soil ($\frac{kg}{m^3}$).

It is assumed that the porosity of the soil in the active layer decreases exponentially as depth increases, which is modeled by the following equation (Sadeghi Chorsi et al., 2024):

$$P(z) = c_0 + c_1 \cdot e^{-c_2 \cdot z}, \qquad (8)$$

where z is the soil depth (m), $P(z)$ is the porosity of the soil at depth z (-), and c_0, c_1, and c_2 are constants that account for soil characteristics of the study area. Soil measurement data for wetlands in the Abisko region captured by Palmtag et al. (2022) at Stordalen Mire was used to calculate values for the constants c_0, c_1, and c_2. Equation 6 was used to calculate sample values for porosity. These porosity sample values were then used to find the best fit for Equation 8 using non-linear least squares, resulting in estimated constant values $c_0 = 0.850$, $c_1 = 0.184$, and $c_2 = 0.055\ m^{-1}$.

The same soil measurement data from Palmtag et al., 2022 was used to calculate sample values for soil saturation using Equation 7. In analysis of the sample saturation values, no clear trend was found in saturation with respect to sample depth. As a result, soil saturation was approximated as the average soil saturation of the samples, as shown in the equation below:

$$S(z) \approx \bar{S} = 0.563, \qquad (9)$$

where z is the soil depth (m), $S(z)$ is the saturation of the soil at depth z (-), and $\bar{S}$ is the average soil saturation (-). These values are used as proxy for the saturation for the study area, given the proximity to the site sample locations and similar vegetation.

Step 4: Active Layer Thickness Estimation

Using the components derived in Steps 1-3, the active layer thickness can be estimated using the following equation (Liu et al., 2012, Schaefer et al., 2015):

$$E = \frac{\rho_w - \rho_i}{\rho_i} \int_0^{ALT} P(z) \cdot S(z)\, dz, \qquad (10)$$

where E is the seasonal vertical surface displacement amplitude (m), z is the depth (m), $P(z)$ is the soil porosity at depth z (-), $S(z)$ is the soil saturation at depth z (-), and ALT

is the active layer thickness (m). P_w is the density of water and ρ_i is the density of ice, which are set to 1000 $\frac{kg}{m^3}$ and 917 $\frac{kg}{m^3}$, respectively.

Using the estimations in Equations 8 and 9, the integral in Equation 10 can be resolved, resulting in the following relationship between E and ALT:

$$E \approx \left(\frac{\rho_w - \rho_i}{\rho_i}\right) \cdot \bar{S} \cdot \left[c_0 \cdot ALT + \left(\frac{c_1}{c_2}\right) \cdot (1 - e^{-c_2 \cdot ALT})\right], \qquad (11)$$

where E is the seasonal vertical surface displacement amplitude (m) and ALT is the active layer thickness (m). c_0, c_1, and c_2 are the constant values derived in Step 3, $\bar{S}$ is the average soil saturation shown in Equation 9, and ρ_w and ρ_i are the densities of water and ice, respectively, as discussed above.

Step 5: Output Data Processing

For each year, the code was run with input points set to the center of each 80 x 80 m pixel of the water-masked interferograms using the steps above. The resulting InSAR ALT estimation values were further processed into a raster which held the ALT value for each pixel in the resolution of the interferograms, 80 x 80 m. The output raster is acceptable to compare against in-situ measurements, due to their similar spatial resolution. However, to address the larger mismatch in scale for comparing the InSAR estimations to the Permafrost_CCI estimations, the InSAR raster was resampled to match the 1 x 1 km scale, allowing for comparison of the data (Khan et al., 2021). The 80 x 80 m resolution InSAR ALT raster was resampled using the bilinear interpolation method, as this is an appropriate method to upscale continuous data (Khan et al., 2021; Singh et al., 2025).

To account for the high landscape variability of the broader study area compared to the in-situ sites, a wetland landcover subset was extracted. The soil parameters used to create the InSAR ALT estimations are wetland specific from Stordalen Mire. By creating this subset, it allows a comparison of the Permafrost_CCI and InSAR ALT estimations solely in an area where the InSAR estimations were more finely tuned. To create this subsection, a buffer was created in ArcGIS around the in-situ sites where the majority of land in the subset is classified as wetland by the Naturvardsverket Land Cover Map (Naturvardsverket, 2025). The buffer is approximately 11 x 3 km around the western sample locations and 8 x 3 km surrounding the eastern sample locations, as seen below in Figure 6. This land cover map was chosen due to the high spatial resolution of 2 x 2 m. Additionally it is produced by the Swedish Environmental Protection Agency and benefits from having locally accurate land cover classes, as compared to more global land cover classification schemas.

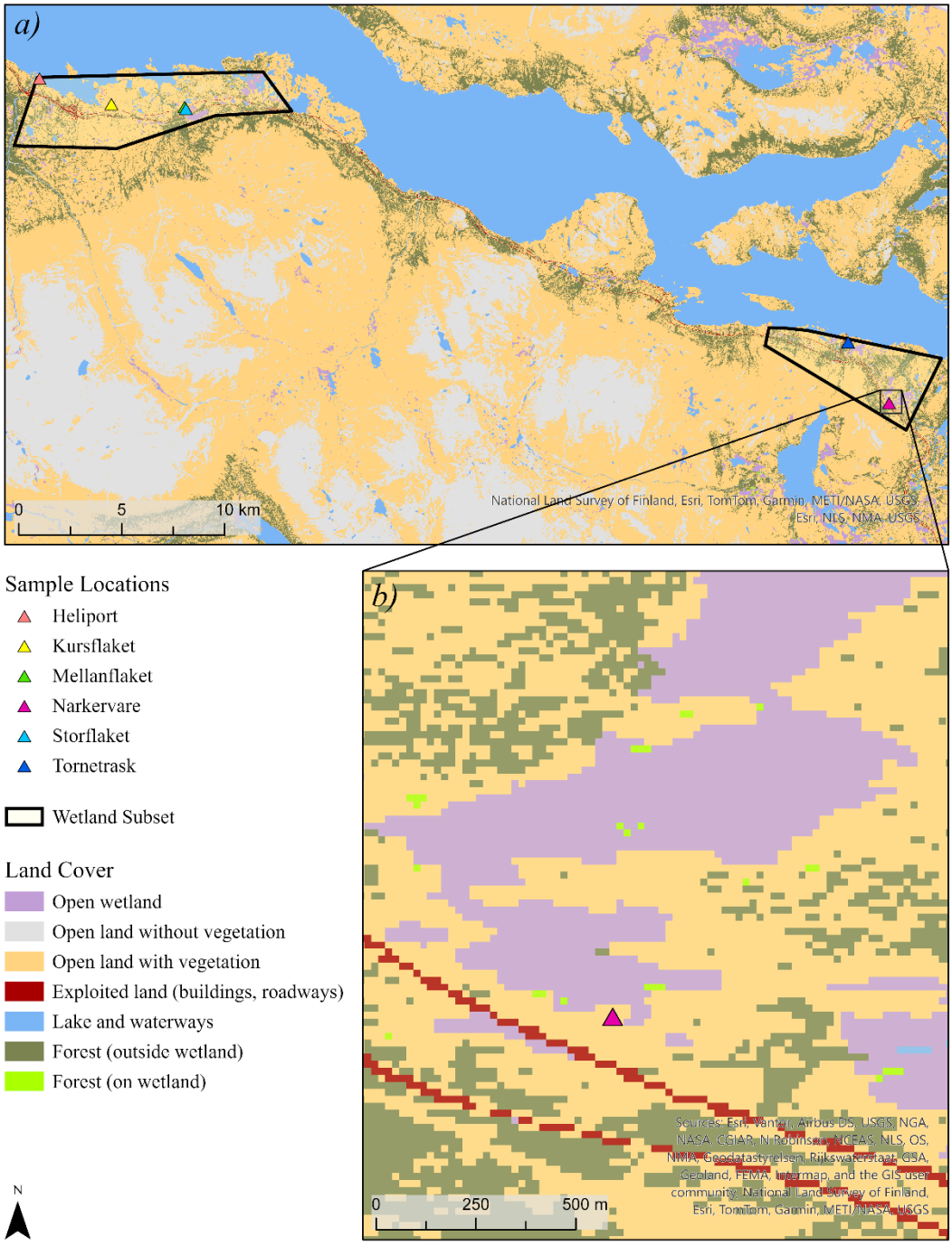

Figure 6: Vegetation map of the study area with the wetland subsets highlighted. In map A the shape and extent of the wetland subset is shown, while map B showcases a zoomed view of site Narkervare surrounded by open wetland and open land with vegetation.

5.4 Evaluation and Uncertainty

To match up the InSAR and in-situ measurements for comparison, the method used by the ESA for the Permafrost_CCI pixel-based match up was used (Westermann et al., 2024b). For each in-situ measurement the closest InSAR pixel was extracted and the

values of each were then paired together for further comparison and used in the following statistics. Following Sadeghi Chorsi et al. (2024) if the sample location was near the border of the InSAR pixel, the adjacent pixel was also chosen, and the mean of these pixels was reported as the InSAR ALT value. For the ALT InSAR estimation and in-situ measurement there is minimal temporal mismatch. Both tactics aim to find the ALT at the maximum depth during the thaw season.

To validate the InSAR ALT estimations produced by this study versus the ground truth data, three metrics were used following the ESA Permafrost_CCI validation method (Westermann et al., 2024b). Bias, absolute bias, and Root Mean Squared Error (RMSE) were calculated, as shown in the following equations:

$$bias = \frac{\sum_{i=1}^{n} (\hat{y}_i - y_i)}{n}, \qquad (12)$$

$$absolute\ bias = \frac{\sum_{i=1}^{n} |(\hat{y}_i - y_i)|}{n}, \qquad (13)$$

$$RMSE = \sqrt{\frac{\sum_{i=1}^{n} (\hat{y}_i - y_i)^2}{n}}, \qquad (14)$$

where n is the number of sample sites, and for each site i, y_i is the ground truth ALT measurement from CALM for that individual sample site (m), and $\hat{y}_i$ is the InSAR-based ALT estimate for that site (m). Bias was used in the Schaefer et al. (2015) study as well to compare in-situ ALT measurements against a remotely sensed ALT estimation. Bias is the mean deviation of the InSAR estimation to the in-situ data. Large deviations in both the positive and the negative direction can cancel out resulting in a bias near 0 (Westermann et al., 2024b). For this reason, absolute bias is also calculated. As shown in Equation 14, RMSE averages the squared difference of the measurement and estimate across sample sites, then takes the square root of that averaged value. The Permafrost_CCI product uses RMSE as the error metric for validation, where an RMSE of less than 0.25 m is acceptable for an ALT that is less than 1.0 meter (Westermann et al., 2024). For an ALT that is thicker than 1.0 meter, the RMSE is ideally lower than 0.5 m.

To evaluate uncertainty for the in-situ measurements, the individual sample points in the CALM grid were used to find the square root of the standard deviation per sample site, which was taken as the individual site uncertainty (Schaefer et al., 2015). The uncertainty ranged from 3.8 – 6.2 cm, depending on the site.

The evaluation of InSAR uncertainty can be propagated by determining the uncertainties and errors within the digital elevation model (DEM), atmospheric artifacts, orbital errors, phase decorrelation, and phase unwrapping errors (Chen et al., 2020). Similar to Chen et al. (2020), Sadeghi Chorsi et al. (2024) and Liu et al. (2012), many of these parameters potential errors were strategically minimized by choosing interferograms with high coherence, low temporal baseline, and low spatial baseline. The atmospheric artifacts were corrected for, described in Section 5.2, however an uncertainty within this correction still exists. The GLO-30 DEM used in the interferogram creation has an uncertainty of ± 0.2m (Simard et al., 2024). Likewise with the ESA's uncertainty metric in the Permafrost_CCI modeling, a full expansive evaluation of the InSAR uncertainty was not possible for this master's thesis. There was not accessible data to perform a full-scale uncertainty error propagation through every input dataset. While an exact number of uncertainty for the InSAR estimations is not available, it is important to note that there will be a level of uncertainty within the results.

6. Results

6.1 Permafrost estimation derived from SAR data

The in-situ measurements for ALT during 2018 – 2023 ranged from 0.65 – 1.5 m while the InSAR estimations ranged from 0.67 – 1.37 m. Figure 7 shows the comparison between the ALT estimated with InSAR using procedures described in Section 5.3 and the ground truth measurements from the six sample locations at CALM site S2. The 1:1 diagonal line represents the ideal scenario where the measured and estimated values would match perfectly. As seen in Figure 7, the points are widely scattered showing a variance among the estimations and measurements. The majority of points lie above the 1:1 line, showing the tendency to overestimate. However, the site with the worst agreement, Torneträsk, has all four estimations significantly under the ideal line. While the InSAR estimations for Kursflaket and Storflaket demonstrated consistent overestimation, both sites showed slight agreement, each having two - three years being closely clustered to the agreement line. Site Heliport was more variable, showing both under and over estimations. Sites Narkervare and Mellanflaket both overestimated four out of six years. Site Mellanflaket demonstrated the best agreement, with five out of six InSAR estimations being within 0.03 – 0.22 m off from the in-situ measurements.

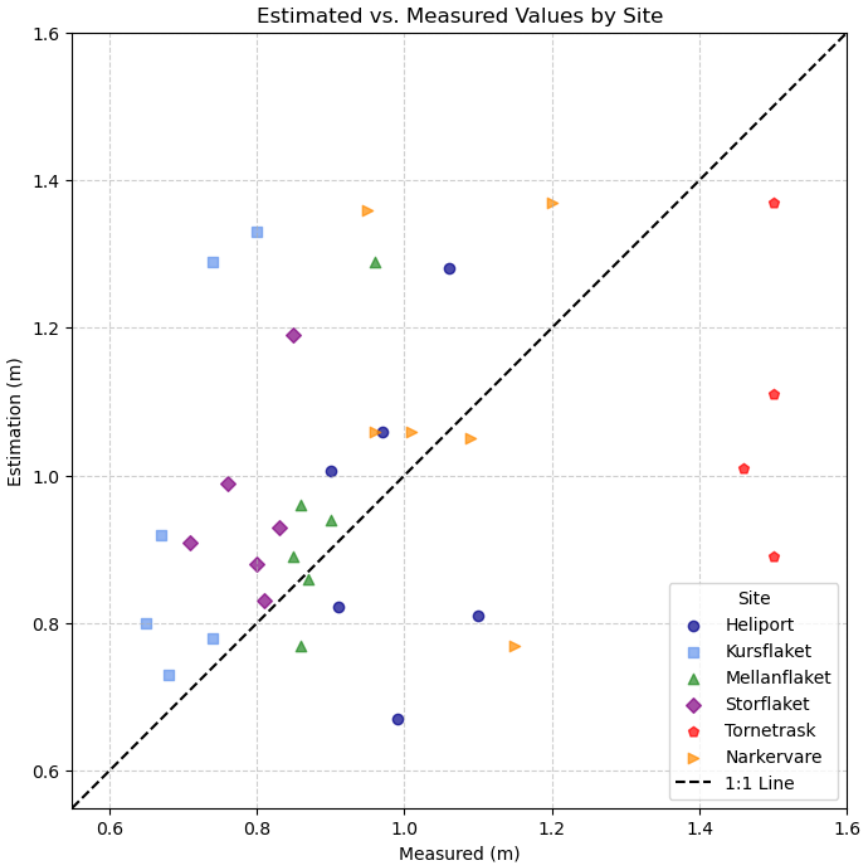

Figure 7: Comparison of measured and estimated ALT at each sample location in CALM site S2. The 1:1 line running diagonally in the graph represents the ideal line where point would lie if they matched exactly.

A time series analysis was performed to investigate the presence of temporal trends. The measured in-situ values are represented with solid lines while the InSAR estimations are represented with dashed lines below in Figure 8. While a lack of precision in the InSAR estimations is visible, there is not a clear temporal trend. In 2023, all of the InSAR estimations are equal to or higher then the actuals, which stands out as the rest of the study years have a mixed range.

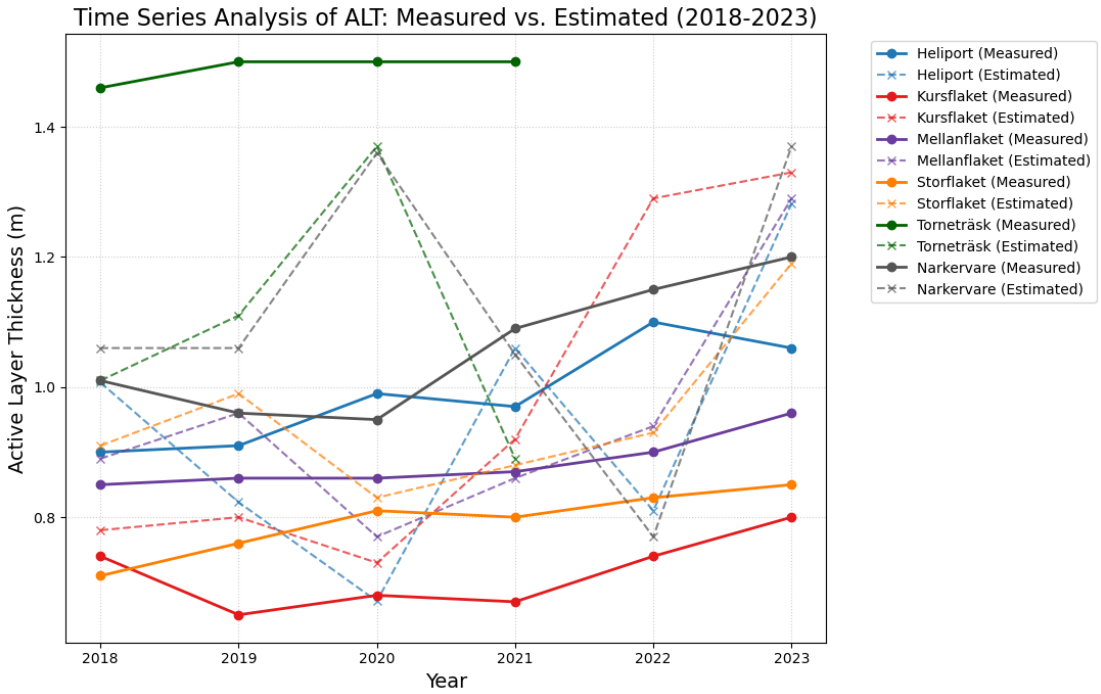

Figure 8: A time series analysis of Active Layer Thickness trends between 2018 and 2023 for the six sample locations of CALM Site S2 (Abisko). Solid lines represent in-situ measurements while the dashed lines represent the InSAR ALT estimations.

Following previous studies Schaefer et al. (2015), Sadeghi Chorsi et al. (2024), Liu et al. (2012) as well as the ESA CCI team, validation metrics of bias, absolute bias, and RMSE were calculated for the study years 2018 - 2023. The resulting metrics are below in Table 4. As seen above in Figure 6 sites Mellanflaket and Storflaket have the closest comparison of ALT estimated and measured values, giving the best agreement. Additionally, these two sites have a lower absolute bias and RMSE. Except for Torneträsk and Kursflaket, all have RMSE values within the acceptable range from the ESA CCI Validation of < 0.25 m.

Table 4: The calculated bias, absolute bias, and RMSE in meters per site for years 2018 – 2023. The exception to this is Torneträsk, as this site only had in-situ data available from 2018 – 2021.

Site	Bias (m)	Absolute Bias (m)	RMSE (m)
Heliport	-0.046	0.186	0.209
Kursflaket	0.262	0.262	0.336
Mellanflaket	0.069	0.101	0.147
Storflaket	0.161	0.161	0.192
Torneträsk	-0.396	0.396	0.432
Narkervare	0.053	0.193	0.245

6.2 Comparison of SAR derived estimation and ESA Permafrost_CCI

The Permafrost_CCI product has produced results for years 1997-2021 at a resolution of 1 x 1 km. Of these years, 2018-2021 are available for a comparison in this study. The Permafrost_CCI product has global coverage in the northern hemisphere, but the Permafrost_CCI Extent product, which estimates likelihood of permafrost in a given area, has a rough boundary near water. For this reason, the areas directly bordering Lake Torneträsk do not have ALT estimates provided by the Permafrost_CCI ALT product.

The ground truth CALM ALT measurements can be directly compared to the Permafrost_CCI ALT estimations, as the ESA CCI team did this during validation (Westermann et al., 2024b). Due to the coarse spatial resolution and the exclusion of areas close to Lake Torneträsk, only three of the six sample locations (Mellanflaket, Storflaket, and Torneträsk) have corresponding Permafrost_CCI values. The CCI ALT values range from 0.46 – 0.50 m in these locations, which are lower compared to the in-situ measurements ranging from 0.71 – 1.5 m.

However, to perform a direct comparison of the InSAR ALT estimates to the Permafrost_CCI ALT estimates, the InSAR rasters were resampled from 80 x 80 m to 1 x 1 km. The CCI ALT estimates are only available for four years of this study, 2018 – 2021 due to CCI data availability. The resampled InSAR estimation, the Permafrost_CCI ALT estimation, the difference between the rasters to show areas of divergence, and the CCI ALT uncertainty are shown below in Figure 7 for 2018. The same information for years 2019 – 2021 is available in Figures S1 – S3 in the appendix.

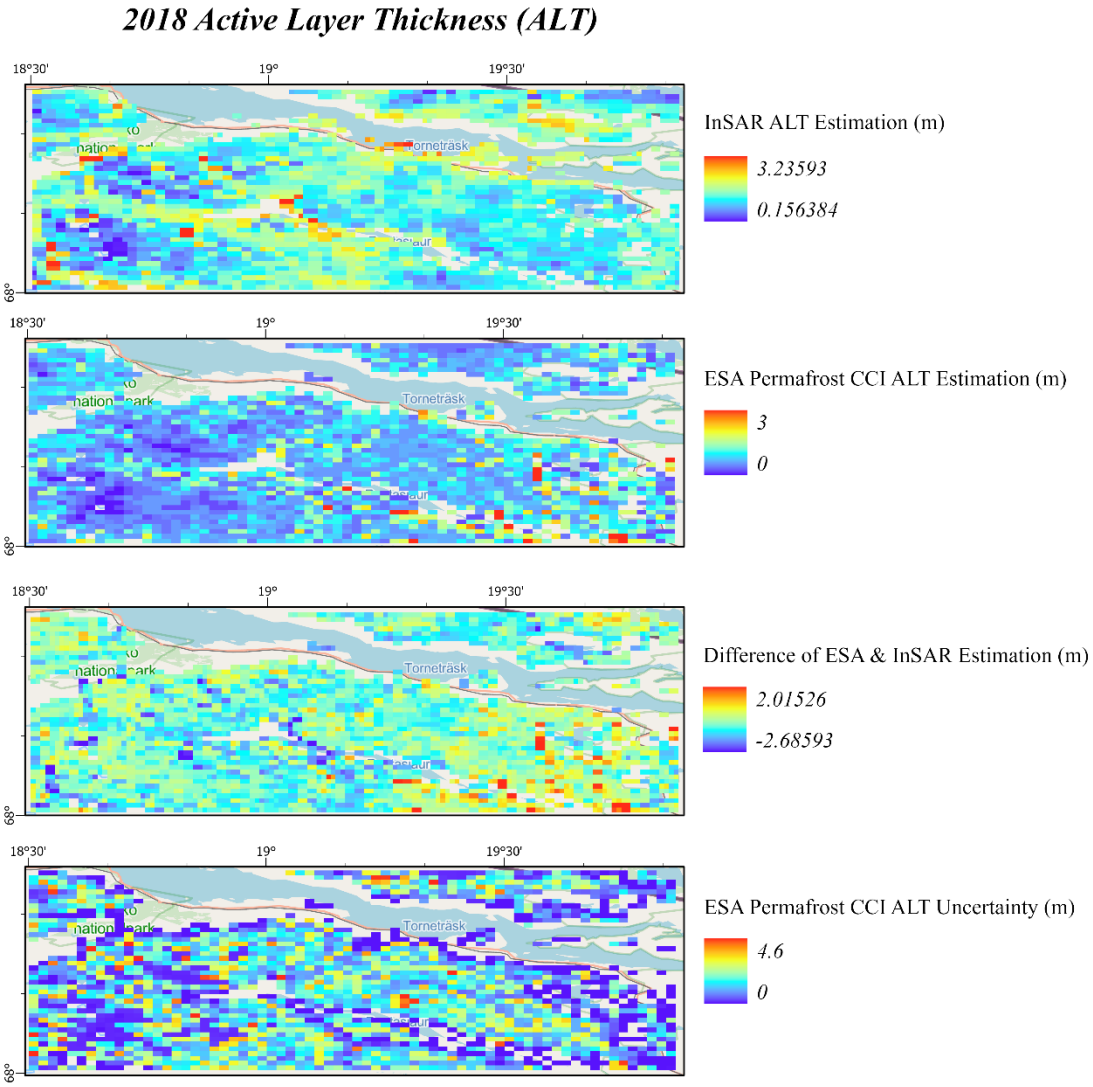

Figure 7: A four part data comparison of InSAR-based ALT, Permafrost_CCI ALT, the difference of the two (Permafrost_CCI – InSAR), and the CCI ALT uncertainty for 2018.

The InSAR ALT estimations in 2018 are largely between 0.75 and 1.3 m along the southern lake front area, shown in the map as a green to light blue color, in the middle of the color ramp. These values fit with the ground truth measurements, as the range for 2018 was 0.75 – 1.46 m. In the southwest corner of the InSAR ALT map, a patch of dark blue with a few blocks of red is visible, indicating low ALT estimates interspersed with a few very high ALT estimates. This area corresponds to a mountainous region and is not expected to be correctly estimated in this study, as the focus of this study was the low wetlands surrounding Lake Torneträsk where ALT estimations can be compared against in-situ measurements. The soil parameters were calculated to reflect that focus. For the InSAR method to perform well in the mountain region, different soil parameters would need to be used. Interestingly, the

Permafrost_CCI ALT estimates the mountain region as having an active layer thickness of zero, with low uncertainty in this area's estimation (Westermann et al., 2024a).

As seen by the difference map in Figure 7, the InSAR and CCI ALT estimates for the year 2018 are close, with most InSAR ALT estimates within one standard deviation of the respective CCI ALT estimate. The estimate difference has a mean of approximately -0.25, meaning that most InSAR ALT estimates are higher than the respective CCI ALT estimate. For 2018, the RMSE between the InSAR ALT and Permafrost_CCI was 0.44 m and the absolute bias was 0.35 m. 2018 maintained the best agreement for Permafrost_CCI and the InSAR estimations. The following three years all had increased errors according to the error metrics, presented in Section 6.3 in Table 5.

6.3 Wetland subset comparison of SAR and Permafrost_CCI

To investigate if vegetation and land cover type had a role in the analysis, the bias, RMSE and absolute bias were calculated for both the entire study area as well as a subset buffering the in-situ measurements. The buffer was approximately 11 x 3 km near the western sample locations and 8 x 3 km on the eastern side of Lake Torneträsk as shown in Figure 6 . The buffer contains landcover of primarily wetland and open land with vegetation as designated by the Naturvardsverket Land Cover Map (Naturvardsverket, 2025). These land covers were chosen due to the sample locations having similar classification in the land cover map. The results of this are below in Table 5.

Table 5: Comparison of years 2018 – 2021 showing Bias, RMSE and Absolute Bias for the total study area and the wetland subset that boundaries the in-situ measurement points.

	Total Study Area			Wetland Subset		
Year	Bias (m)	RMSE (m)	Absolute Bias(m)	Bias (m)	RMSE (m)	Absolute Bias(m)
2018	0.19	0.44	0.35	0.06	0.24	0.13
2019	0.86	0.92	0.79	0.10	0.31	0.17
2020	0.31	0.56	0.40	0.16	0.40	0.22
2021	0.28	0.53	0.38	0.19	0.44	0.24

As seen in by the error metrics in Table 5, restricting the study area to the wetland subset greatly improves accuracy as compared to the total study area. The RMSE is reduced by 50 – 60%. A large spike in the error metrics is shown for the total study area in 2019 as compared to other years of the study. Refining the area to the wetlands reduce these errors, suggesting an anomaly occurring outside the wetlands.

7. Discussion

7.1 InSAR Active Layer Thickness Estimation

Numerous studies have shown how permafrost degradation, warming trends, and active layer thickening have been concurrent in the artic region (Åkerman & Johansson, 2008; Gangodagamage et al., 2014; Liu et al., 2012; Sadeghi Chorsi et al., 2024; Strand et al., 2020). Sadeghi Chorsi et al. (2024) found a maximum RMSE of approximately 0.20 m in their InSAR estimation of ALT in a continuous permafrost. This is lower in comparison to this Master's thesis results which had the highest RMSE of 0.43 m for Torneträsk site and 0.34 for Kursflaket site. The rest of the study sites had a lower RMSE of 0.15 – 0.25 m. While the Sadeghi Chorsi et al. (2024) study and this thesis investigate different permafrost zones, we both found RMSE within the ESA validation standard.

The final two years of this study have larger variation in values then the previous years (can be found in Appendix Table 1 – 5). While the entire reason for these higher values in 2022 and 2023 is unknown, a likely partial cause is the reduced number of interferograms available for the years 2022 and 2023 due to the loss of Sentinel-1B data. Only nine interferograms were available for use during these years thaw seasons- The frequency of interferograms spread over the thaw season is necessary to capture the changing active layer thickness that is attributed to surface subsidence.

Performing InSAR ALT estimation on a continuous permafrost zone has proven successful using this methodology in northern Alaska and Canada, where the permafrost region has similar soil characteristics and features throughout (Liu et al., 2012; Sadeghi Chorsi et al., 2024). However, performing the same method used in the continuous zone proved challenging in Abisko. Permafrost underlies a very small extent of the study area and is considered somewhere between a sporadic and isolated patches zone (Obu et al., 2019). A key factor to successfully running the method is utilizing accurate soil characteristic values for porosity and saturation, as well as accurate surface temperature readings. Considering the high variability of vegetation and topography in the study area, the InSAR estimations are more accurate in the areas with similar vegetation and soil characteristics as the sample locations and Stordalen mire, where the soil measurements were taken. It can be concluded that the more homogenous the region, the better that ALT will be estimated, given how this method utilizes a single porosity and saturation calculation for the entire region. Additionally, a limitation is that while the results benefited from having local values, there is still spatial variability that is lost when only using one location's soil characteristic. However, as with many remote sensing topics, the best available proxy was utilized.

The sporadic and patchy nature of the permafrost in this area leads to high spatial variability and complicates validation efforts. While permafrost does not underlie the entire study area, an ALT estimation is provided for each pixel in the study area. This is due to ALT being estimated by surface motion and displacement, which can happen in areas with seasonal thaw, even if not underlain by permafrost. While small areas estimated an ALT of zero, most areas had at least some active layer thickness indication generated. Labeling this as ALT can be misleading, as ALT by definition only occurs in permafrost areas (Harris et al., 1998). Thaw in non-permafrost areas is a seasonal environmental process, especially in northern latitudes.

The estimation code used in this study relies on several factors to produce accurate results, such as the chosen thaw season start and end dates being correct, soil porosity and saturation variables being accurate for each location, and interferograms being corrected for as much noise as possible (Liu et al., 2012; Sadeghi Chorsi et al., 2024). This study emphasizes the necessity of performing atmospheric corrections for all interferograms used. The estimation code was run prior to atmospheric corrections as a test, and the resulting ALT estimations were consistently off by about 70 - 120 cm, which is significant. After performing the corrections, the estimated values were in a more reasonable error range (< 32 cm) when compared with the in-situ values.

Previous studies have cited several causes of decorrelation in InSAR phase measurements and coherence, which can lead to inaccurate resulting data. Measurements in mountainous areas where vegetation growth and rapidly changing elevation occur can cause decorrelation (Xu et al., 2021). Additionally, decorrelation can be caused by measurements made in close proximity to standing water (Liu et al., 2015). Northern Sweden has many bodies of water surrounded by mountainous regions, especially in this study area, including Torneträsk Lake and the Norwegian Sea. This amplifies the need to apply a water mask and check the coherence values for each interferogram before processing. However not all water can be accounted for in the water mask as the lowland of the area has waterlogged vegetation areas such as fen and bogs. The presence of this water could account for some of the unwrapping errors.

Using the ASF Vertex tool was helpful in creating the interferograms used in this study, as it made searching for the temporal and spatial baselines easy. However, if more control over the reference point is desired, it is better to use a tool like SNAP, which is the ESA product for producing interferograms. This allows more control over the reference point, which is especially useful if doing a time series analysis.

7.2 ESA Permafrost_CCI - Active Layer Thickness Estimation Product

Overall, the Permafrost_CCI ALT product has a similar pattern to the InSAR based estimations, more so in areas where the soil characteristics likely match the truth measurements from Stordalen mire due to land cover type. As shown in Table 5, the bias for the total study area ranges from 0.19 – 0.86 m depending on the year. The RMSEs however are quite large ranging from 0.44 – 0.92 m, due to the large range of differences that occur between mismatched estimations between Permafrost_CCI and the InSAR estimations. This is also visible in the difference maps for each year, as there are zones where the models estimated the ALT completely differently. The two estimation models diverged in each year in the mountainous regions to the southeast of Lake Torneträsk. Interestingly, the Permafrost_CCI ALT estimates low active layer thickness values in the mountainous region, while the ground truth measurements taken in the mountains were consistently at 1.12 m or higher since year 2000 (CALM, Westermann et al., 2024c). These measurements stopped being reported in 2012 for an unknown reason. The Permafrost_CCI Extent map indicates a high level of permafrost in the mountain areas, as well as the permafrost zonal index map by Obu et al. (2019), which labels the higher mountain regions as discontinuous permafrost, surrounded by sporadic areas. The InSAR estimations indicate high ALT in this region, but as they have different soil characteristics not accounted for in this study, these estimations cannot be relied on.

Spatial resolution mismatch is a problem with the Permafrost_CCI, as the product covers a 1 x 1 km area of surface for each estimated value, while the InSAR-derived estimations cover 80 x 80 m. Upscaling the InSAR estimations removes the more granular detail that is provided with a finer resolution. The coarse spatial resolution glosses over the spatial variability that occurs at small scales throughout the landscape (Liu et al., 2012). Active layer thickness, extent, and ground temperature can all dramatically change within a 1 x 1 km area represented by a single CCI product grid cell. Multiple studies show that ALT has large spatial variations within areas smaller than 1 km^2 (Gomersall & Hinkel, 2001; Hinkel & Nelson, 2003; Liu et al., 2012). The spatial resolution of Permafrost_CCI is constrained by the resolution of the MODIS land surface temperature product, which accounts its relatively coarse scale (Westermann et al., 2024a). However, given that ALT has large variability in areas this size, it calls into question the potential accuracy and validity of the Permafrost_CCI dataset. The product validation report for Permafrost_CCI cites a median bias of 13 cm for ALT (Westermann et al., 2024b). This validation occurs mainly in the arctic, concentrated in Northern American continuous permafrost zones which coincides with the majority of available in-situ data measurements. This means the validation is

skewed for continuous permafrost zones and might not be as accurate for different categorized zones, such as Abisko (Westermann et al., 2024b).

A potential reason for misalignment with the InSAR ALT estimations and the Permafrost_CCI estimations is the slight temporal mismatch. Both estimations are meant to capture maximum seasonal thaw depth as this is the active layer thickness. However, due to Permafrost_CCI extremely large extent (Northern Hemisphere) simplifications or generalizations have been made which may not ideally apply to every location covered by the extent. The temporal resolution of the Permafrost_CCI is annual at maximum thaw depth, but the metadata also lists this time frame as July – August (Westermann et al., 2024a). While this may be the time of maximum thaw depth for places in North America, in Abisko this does not happen until second or third week of September when the CALM site measurements are taken. The temporal mismatch could be the cause of variations between the InSAR ALT estimates and the Permafrost_CCI estimates.

Additionally, half of the ground truth sites are not calculated in the Permafrost_CCI product. This is due to the fact that the Permafrost_CCI ALT estimations are in part based on another product in the Permafrost_CCI package called Permafrost Extent. In this extent, the three sample locations of Heliport, Kursflaket, and Narkervare are set to 0, meaning no permafrost in the area according to the model, when in fact permafrost does exist in these areas. This information in turn feeds the ALT estimation, which does not perform calculations on an area where there is believed to be no permafrost (Westermann et al., 2024a). This is likely due to these sites being in close proximity to Torneträsk Lake, which would not have permafrost. Due to the coarse spatial resolution and large area covered, it sets the permafrost extent on the surface surrounding the lake to 0, even if it does have existing permafrost, such as in 4 of the sample locations that are missed by the CCI ALT product. This is a downside to using such a coarse spatial resolution, especially in a non-continuous permafrost zone where the values cannot be easily interpolated. The permafrost extent product looks to be heavily influenced by

elevation, as the areas with high permafrost extent are also areas with high elevation, according to the DEM comparison in Figure 8 below.

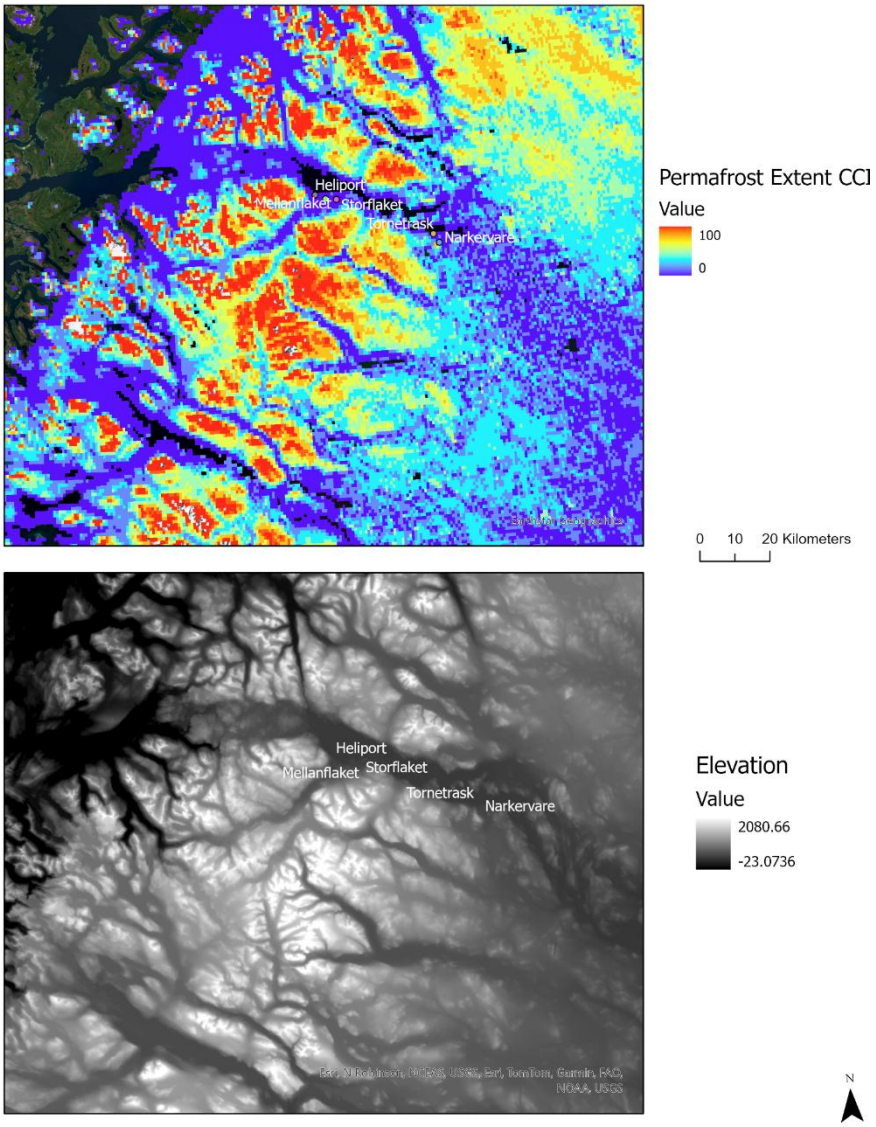

Figure 8 - Comparison of Permafrost_CCI Extent product and digital elevation model (Copernicus DEM GLO-30) to identify patterns of similarity.

Some inaccuracies in the ESA product can be attributed to issues with the scale and resolution. This product does not have the ability to handle subtle fluctuations in the landscape, as the resolution is too coarse. However, Permafrost_CCI does produce a large-scale global coverage for the northern hemisphere. This is useful for general trends and high-level analysis. Depending on the needs of the research, it is useful to have multiple options to investigate similar processes. For instance, a study doing global trend analysis on decades of permafrost projections does not need to deal with the fine details the InSAR-derived product can offer. However, a study focusing on regional and local trends or how degradation will affect a very specific area would benefit from the InSAR-derived product.

7.3 Wetland subset and land cover

The wetland subset improved accuracy when comparing the InSAR estimations to the Permafrost_CCI in the study area. These results demonstrate how land cover can affect the estimations. As previously stated, the InSAR ALT estimations rely on soil moisture information, such as porosity and saturation, which greatly affect the results. The soil information used in this study came from samples at Stordalen mire in the wetlands. Soil moisture is greatly varied in the study area, ranging from waterlogged peat bogs and fens compared to the drier soil in the southern lowlands or mountainous region, laying outside of the wetland. By analyzing a smaller subset where the soil parameters match closely to the parameters used in the ALT estimation equation, this allows for a more direct comparison. Additionally, this analysis showcases how land cover, soil moisture, and spatial heterogeneity play a role in ALT estimation.

7.4 Limitations and recommendations for future studies

This study has several limiting factors, including sample size of truth data, heavy reliance on soil information, and spatial mismatch amongst all the comparison datasets. Given the extremely small ground truth sample size, the ability to validate the InSAR estimations was limited to a small area. This is a frequent hurdle in the remote sensing community, especially for studying permafrost as ground truth measurements are limited. Additionally, uncertainty was not able to be calculated in depth for the interferograms. Quantifying the uncertainties associated with InSAR would constitute a valuable part of a future study.

The main objective of this study was to estimate ALT with remote sensing techniques as a way of supplementing scarce in-situ measurements. However, the small amount of truth data available did affect the scope of validation in this study, which could be further improved and be more statistically significant with more data points. A limited sample size can create a spatial bias when the in-situ measurements contain similar soil and environmental traits. While this may be acceptable for a continuous permafrost zone, it adds complexity to the validation of an area with sporadic permafrost and significant spatial variation. Furthermore, the way the original methodology from Sadeghi Chorsi et al. (2024) handles soil characteristics is a limitation for studying a heterogeneous landscape. The utilization of a single metric for soil saturation and porosity in a transitional permafrost zone with varied topography is not optimal. Additionally, a limitation of this study is the spatial resolution mismatch that occurs between sample locations, InSAR estimates, and the Permafrost_CCI product. Resampling the InSAR data to fit into the Permafrost_CCI specifications reduces the granularity of the InSAR estimations.

One recommendation for future studies is to investigate a sporadic area with more ground truth measurements and locations, as this would allow for a more in-depth validation effort of the area. Additionally, an update or overhaul of the Sadeghi Chorsi et al. (2024) method allowing for more variability within the soil characteristics used in calculations would improve large-scale ALT estimations. The ESA CCI team had similar limitations in their validation and called for a more robust modeling need for areas with snow regimes and sub ground properties (Westermann et al., 2024b). This would allow for different areas, such as mountainous regions, to be better evaluated, which would potentially allow this method to produce more accurate results for sporadic permafrost areas.

8. Conclusions

Active layer thickness is a key indicator of the thaw trend of permafrost. While ground measurements have high accuracy, they are limited in spatial coverage (Liu et al., 2012). To gain a wider knowledge of the impacts of permafrost degradation, it is necessary to establish a process to efficiently estimate the active layer thickness at a large scale. The aim of this Master's thesis was to estimate the active layer thickness in Abisko, Sweden using InSAR techniques, as well as evaluate and compare the InSAR estimations to ground truth data and the Permafrost_CCI ALT product.

In comparison to the in-situ measurements, the InSAR estimations had an average RMSE of 0.26 m, an average difference of 0.15 m, and an average absolute bias of 0.22 m across the study years. Evaluating the Permafrost_CCI ALT product against the InSAR estimations reveals the extent of agreement and divergence between the two estimation methods. The average difference over the entire study region when comparing these two products was 0.41 m. When investigating a smaller region with wetland land cover similar to the sample locations, the average difference reduces to 0.12.

The application of InSAR to active layer thickness estimation in the Abisko region presented significant challenges, primarily due to the heterogeneous nature of the permafrost distribution. The method used by Sadeghi Chorsi et al. (2024) was originally developed and utilized for continuous permafrost zones with uniform soil and vegetation characteristics, exhibited lower accuracy when applied to a sporadic permafrost zone. While InSAR produced accurate estimates in smaller subsections of the study area, the overall performance varied with the terrain of the study area. When evaluating the broader area of the study region, the mountainous regions are not correctly estimated due to the method's reliance on a single model for soil porosity and

saturation across the entire estimated area, which is a limitation for using this method on a variable landscape.

The InSAR estimations roughly align with the general pattern observed in the Permafrost_CCI ALT estimations, except for the mountainous areas to the south of Lake Torneträsk, for which InSAR results both under- and over-estimated as compared to the Permafrost_CCI estimates, depending on the year. However, the InSAR estimations were able to produce active layer thickness values within range of the in-situ ground measurements for similar land covers in the study area.

References

Åkerman, H. J., & Johansson, M. (2008). Thawing permafrost and thicker active layers in sub-arctic Sweden. *Permafrost and Periglacial Processes*, 19(3), 279–292. https://doi.org/10.1002/ppp.626

Alaska Satellite Facility. (n.d.). HyP3 Product Guide. Retrieved August 18, 2025, from https://hyp3-docs.asf.alaska.edu/guides/insar_product_guide/

Altman, D. G., & Bland, J. M. (2005). Standard deviations and standard errors. BMJ, 331(7521), 903. https://doi.org/10.1136/bmj.331.7521.903

Bamler, R., & Hartl, P. (1998). Synthetic aperture radar interferometry. *Inverse Problems*, *14*(4), R1. https://doi.org/10.1088/0266-5611/14/4/001

Chen, J., Wu, Y., O'Connor, M., Cardenas, M. B., Schaefer, K., Michaelides, R., & Kling, G. (2020). Active layer freeze-thaw and water storage dynamics in permafrost environments inferred from InSAR. *Remote Sensing of Environment*, *248*. https://doi.org/10.1016/j.rse.2020.112007

Circumpolar Active Layer Monitoring (CALM). Retrieved from https://www2.gwu.edu/~calm/data/north.htm. Last accessed August 15 2025.

Clayton, L. K., Schaefer, K., Battaglia, M. J., Bourgeau-Chavez, L., Chen, J., Chen, R. H., Chen, A., Bakian-Dogaheh, K., Grelik, S., Jafarov, E., Liu, L., Michaelides, R., Moghaddam, M., Parsekian, A., Rocha, A., Schaefer, S., Sullivan, T., Tabatabaeenejad, A., Wang, K., Wilson, C., Zebker, H., Zhang, T., & Zhao, Y. (2021). Active layer thickness as a function of soil water content. *Environmental Research Letters*, 16(5). https://doi.org/10.1088/1748-9326/abfa4c

Copernicus Program. (n.d.). *S1 mission*. Retrieved from https://sentiwiki.copernicus.eu/web/s1-mission

Copernicus Climate Change Service, Climate Data Store (C3S), (2022): In-situ observations of water vapour and atmospheric delay from the groud-based GNSS network from 1996 onward. Copernicus Climate Change Service (C3S) Climate Data Store (CDS). DOI: 10.24381/cds.34a04494 Last accessed March 20, 2025.

Copernicus Climate Change Service, Climate Data Store, (2023): ERA5 hourly data on pressure levels from 1940 to present. Copernicus Climate Change Service (C3S) Climate Data Store (CDS), DOI: 10.24381/cds.bd0915c6 Last accessed March 20, 2025.

Du, R., Peng, X., Frauenfeld, O. W., Jin, H., Wang, K., Zhao, Y., Luo, D., & Mu, C. (2023). Quantitative impact of organic matter and soil moisture on permafrost. Journal of Geophysical Research: Atmospheres, 128(3). https://doi.org/10.1029/2022JD037686

Foody, G. M. (2024). Ground Truth in Classification Accuracy Assessment: Myth and Reality. Geomatics, 4(1), 81–90. https://doi.org/10.3390/geomatics4010005

Gangodagamage, C., Rowland, J. C., Hubbard, S. S., Brumby, S. P., Liljedahl, A. K., Wainwright, H., Wilson, C. J., Altmann, G. L., Dafflon, B., Peterson, J., Ulrich, C., Tweedie, C. E., & Wullschleger, S. D. (2014). Extrapolating active layer thickness measurements across Arctic polygonal terrain using LiDAR and NDVI data sets. *Water Resources Research*, 50(8), 6339-6357. https://doi.org/10.1002/2013WR014283

Goldstein, R. M., & Werner, C. L. (1998). Radar interferogram filtering for geophysical applications. Geophysical Research Letters, 25(21), 4035–4038. https://doi.org/10.1029/1998GL900033

Gomersall, C. E., & Hinkel, K. M. (2001). Estimating the variability of active-layer thaw depth in two physiographic regions of northern Alaska. Geographical Analysis, 33(2), 141–155. https://doi.org/10.1111/j.1538-4632.2001.tb00441.x

Gruber, S. (2012). Derivation and analysis of a high-resolution estimate of global permafrost zonation. *The Cryosphere*, 6, 221-233. https://doi.org/10.5194/tc-6-221-2012

Guan, S., Wang, C., Tang, Y., Zou, L., Yu, P., Li, T., & Zhang, H. (2024). North American Circum-Arctic Permafrost Degradation Observation Using Sentinel-1 InSAR Data. Remote Sensing, 16(15), 2809. https://doi.org/10.3390/rs16152809

Harris, S., French, H., Heginbottom, J., Johnston, G., Ladanyi, B., Sego, D., & Everdingen, R.. (1988). *Glossary of permafrost and related ground-ice terms*. National Research Council of Canada, Associate Committee on Geotechnical Research. https://doi.org/10.4224/20386561

Hinkel, K. M., & Nelson, F. E. (2003). Spatial and temporal patterns of active layer thickness at Circumpolar Active Layer Monitoring (CALM) sites in northern Alaska, 1995–2000. Journal of Geophysical Research: Atmospheres, 108(D2), 4057. https://doi.org/10.1029/2001JD000927

Hogenson, K., Kristenson, H., Kennedy, J., Johnston, A., Rine, J., Logan, T., Zhu, J., Williams, F., Herrmann, J., Smale, J., & Meyer, F. (2020). Hybrid Pluggable Processing Pipeline (HyP3): A cloud-native infrastructure for generic processing of SAR data (v0.9.13). Zenodo. https://doi.org/10.5281/zenodo.14728051

ICOS Sweden, Lundin, E., Meire, A., Rakos, N. (2023). Ecosystem eco time series (ICOS Sweden) from Abisko-Stordalen Palsa Bog, 2018-12-31–2019-12-31, Swedish National Network, https://hdl.handle.net/11676/oe82doh93tVyx69tbimyQTV-. Date downloaded August 8, 2025.

ICOS Sweden, Lundin, E., Meire, A., Rakos, N. (2023). Ecosystem eco time series (ICOS Sweden) from Abisko-Stordalen Palsa Bog, 2019-12-31–2020-12-31, Swedish National Network, https://hdl.handle.net/11676/VFSWXiJQrmK9D72U9Lwa3J2H. Date downloaded August 8, 2025.

ICOS Sweden, Lundin, E., Meire, A., Rakos, N. (2023). Ecosystem eco time series (ICOS Sweden) from Abisko-Stordalen Palsa Bog, 2020-12-31–2021-12-31, Swedish National Network, https://hdl.handle.net/11676/kLrds4v3qu1skv6W_hAGX78i. Date downloaded August 8, 2025.

ICOS Sweden, Lundin, E., Meire, A., Rakos, N. (2023). Ecosystem eco time series (ICOS Sweden) from Abisko-Stordalen Palsa Bog, 2021-12-31–2022-12-31, Swedish National Network, https://hdl.handle.net/11676/4pkE5pGz8cWvQozGLp3cmzh3. Date downloaded August 8, 2025.

Jasoliya, D., Untaroiu, A., & Untaroiu, C. (2024). A review of soil modeling for numerical simulations of soil-tire/agricultural tools interaction. *Journal of Terramechanics*, *111*, 41–64. https://doi.org/10.1016/j.jterra.2023.09.003

Johansson, M., Åkerman, H., Keuper, F., Christensen, T.R., Lantuit, H., & Callaghan, T.V. (2011). Past and present permafrost temperatures in the Abisko area: Redrilling of boreholes. Ambio, 40(6), 558–565. https://doi.org/10.1007/s13280-011-0163-3

Jolivet, R., Grandin, R., Lasserre, C., Doin, M.-P., & Peltzer, G. (2011). Systematic InSAR tropospheric phase delay corrections from global meteorological reanalysis data. Geophysical Research 1 Letters, 38(17). https://doi.org/10.1029/2011GL048757

Jolivet, R., Agram, P. S., Lin, N. Y., Simons, M., Doin, M.-P., Peltzer, G., & Li, Z. (2014). Improving InSAR geodesy using Global Atmospheric Models. *Journal of Geophysical Research: Solid Earth.* 119(2), 1799–1820. https://doi.org/10.1002/2013JB010588

Khan, M. A. R., Singh, S., Pandey, P., Bhardwaj, A., Ali, S. N., Chaturvedi, V., & Ray, P. K. C. (2021). Modelling Permafrost Distribution in Western Himalaya Using Remote Sensing and Field Observations. Remote Sensing, 13(21), 4403. https://doi.org/10.3390/rs13214403

Lantmateriet, Sweden Boundary Map. Data downloaded April 2, 2025.

Lakshmiprasad, R. B., Peth, S., Woche, S. K., & Graf, T. (2024). New Method for Hydraulic Characterization of Variably Saturated Zone in Peatland-Dominated Permafrost Mires. Land, 13(12), 19-90. https://doi.org/10.3390/land13121990

Liu, L., Schaefer, K., Zhang, T., & Wahr, J. (2012). Estimating 1992–2000 average active layer thickness on the Alaskan North Slope from remotely sensed surface subsidence. Journal of Geophysical Research: Earth Surface, 117(F1). https://doi.org/10.1029/2011JF002041

Liu, L., Schaefer, K. M., Chen, A. C., Gusmeroli, A., Zebker, H. A., & Zhang, T. (2015). Remote sensing measurements of thermokarst subsidence using InSAR. *Journal of Geophysical Research: Earth Surface*, 120(9), 1935-1948.

Lundin, E., Crill, P., Grudd, H., Holst, J., Kristoffersson, A., Meire, A., Molder, M., Rakos, N. (2025). ETC L2 Meteosens from Abisko-Stordalen Palsa Bog, 2021-12-31–2024-12-31, ICOS RI, https://hdl.handle.net/11676/smHPUALxQBvuuMi0Rnu_c0RQ Date downloaded August 8, 2025.

Meng, L., Yan, C., Lv, S., Sun, H., Xue, S., Li, Q., Zhou, L., Edwing, D., Edwing K., Geng, X., Wang, Y., Yan, X-H. (2024). Synthetic aperture radar for geosciences. Reviews of Geophysics,62. http://doi.org/10.1029/2023RG000821

Meyer, Franz. "Spaceborne Synthetic Aperture Radar – Principles, Data Access, and Basic Processing Techniques." SAR Handbook: Comprehensive Methodologies for Forest Monitoring and Biomass Estimation. Eds. Flores, A., Herndon, K., Thapa, R., Cherrington, E. NASA. 2019. https://doi.org/10.25966/nr2c-s697

Michaelides, R. J., Schaefer, K., Zebker, H. A., Parsekian, A., Liu, L., Chen, J., Natali, S., Ludwig, S., & Schaefer, S. R. (2019). Inference of the impact of wildfire on permafrost and active layer thickness in a discontinuous permafrost region using the remotely sensed active layer thickness (ReSALT) algorithm. Environmental Research Letters, 14(3). https://doi.org/10.1088/1748-9326/aaf932

Mishra, U., Hugelius, G., Shelef, E., Yang, Y., & Orr, A. (2021). Spatial heterogeneity and environmental predictors of permafrost region soil organic carbon stocks. *Science Advances*, 7(9). https://doi.org/10.1126/sciadv.aaz5236

Naturvårdsverket (Swedish Environmental Protection Agency). (2025, January 8). National Land Cover Database (NMD). https://www.naturvardsverket.se/en/services-and-permits/maps-and-map-services/national-land-cover-database/. Data downloaded August 5, 2025.

Nelson, F., Brown, J., Lewkowicz, T., & Taylor, A. (1996). Active layer protocol. In U. Molau & P. Mølgaard (Eds.), ITEX Manual: A practical guide to the International Tundra Experiment (2nd ed., pp. 14–16). Danish Polar Center.

Obu, J. (2021). How much of the Earth's surface is underlain by permafrost? Journal of Geophysical Research: EarthSurface, 126. https://doi.org/10.1029/2021JF006123

Obu, J., Westermann, S., Bartsch, A., Berdnikov, N., Christiansen, H. H., Dashtseren, A., Delaloye, R., Elberling, B., Etzelmüller, B., Kholodov, A., Khomutov, A., Kääb, A., Leibman, M. O., Lewkowicz, A. G., Panda, S. K., Romanovsky, V., Way, R. G., Westergaard-Nielsen, A., Wu, T., Yamkhin, J., Zou, D. (2019). Northern Hemisphere permafrost map based on TTOP modelling for 2000–2016 at 1 km2 scale. Earth-Science Reviews, 193, 299–316. https://doi.org/10.1016/j.earscirev.2019.04.023

Palmtag, J., Obu, J., Kuhry, P., Siewert, M., Weiss, N., Gustaf, G. (2022). Detailed pedon data on soil carbon and nitrogen for the northern permafrost region. Dataset version 1. Bolin Centre Database. https://doi.org/10.17043/palmtag-2022-pedon-1

Pedron, S. A., Jespersen, R. G., Xu, X., Khazindar, Y., Welker, J. M., & Czimczik, C. I. (2023). More snow accelerates legacy carbon emissions from arctic permafrost. AGU Advances, 4(4). https://doi.org/10.1029/2023AV000942

Rouyet, L., Bolch, T., Brardinoni, F., Caduff, R., Cusicanqui, D., Darrow, M., Delaloye, R., Echelard, T., Lambiel, C., Pellet, C., Ruiz, L., Schmid, L., Sirbu, F., and Strozzi, T.: Rock Glacier Inventories (RoGIs) in 12 areas worldwide using a multi-operator consensus-based procedure, Earth Syst. Sci. Data, 17, 4125–4157. https://doi.org/10.5194/essd-17-4125-2025

Riseborough, D. (2003). Thawing and freezing indices in the active layer. In Proceedings of the 8th International Conference on Permafrost (Vol 2, 953-958). AA Balkema.

Sadeghi Chorsi, T., Meyer, F. J., & Dixon, T. H. (2024). Toward long-term monitoring of regional permafrost thaw with satellite interferometric synthetic aperture radar. The Cryosphere, 18(9), 3723–3740. https://doi.org/10.5194/tc-18-3723-2024

Schaefer, K., Liu, L., Parsekian, A., Jafarov, E., Chen, A., Zhang, T., Gusmeroli, A., Panda, S., Zebker, H. A., & Schaefer, T. (2015). Remotely Sensed Active Layer Thickness (ReSALT) at Barrow, Alaska Using Interferometric Synthetic Aperture Radar. *Remote Sensing*, 7(4), 3735-3756. https://doi.org/10.3390/rs70403735

Seemann, F., & Sannel, A. B. K. (2024). Morphology and dynamics of thermokarst ponds in a sub-arctic permafrost peatland, northern Sweden. Earth Surface Processes and Landforms, 49(15), 4883–5405. https://doi.org/10.1002/esp.6021

Simard, M., Denbina, M., Marshak, C., & Neumann, M. (2024). A global evaluation of radar-derived digital elevation models: SRTM, NASADEM, and GLO-30. Remote Sensing of Environment, 295. https://doi.org/10.1016/j.rse.2023.113678

Simons, M., & Rosen, P. A. (2007). Interferometric Synthetic Aperture Radar Geodesy. In G. Schubert (Ed.), Treatise on Geophysics (391–446). https://doi.org/10.1016/B978-044452748-6.00059-6

Singh, A., Shrestha, D., Ghimire, K., Mishra, S., Rana, D., & Acharya, S. (2025). Assessing machine learning models to generate permafrost distribution map in Solukhumbu, Nepal. Geodesy and Geodynamics, 3, 275-287. https://doi.org/10.1016/j.geog.2024.08.003

Sjögersten, S., Ledger, M., Siewert, M., de la Barreda-Bautista, B., Sowter, A., Gee, D., Foody, G., and Boyd, D. S (2023) Optical and radar Earth observation data for upscaling methane emissions linked to permafrost degradation in sub-Arctic peatlands in northern Sweden, Biogeosciences, 20, 4221–4239, https://doi.org/10.5194/bg-20-4221-2023

Smith, E. K., & Weintraub, S. (1953). The Constants in the Equation for Atmospheric Refractive Index at Radio Frequencies. Proceedings of the IRE, 41, 1035-1037. https://doi.org/10.1109/JRPROC.1953.274297

Stimmler, P., Obst, M., Stein, M., Goeckede, M., Hockmann, K., & Schaller, J. (2023). Silicon and calcium controls on iron and aluminum mobility in Arctic soils. *Chemosphere*, *335*, 139087. https://doi.org/10.1016/j.chemosphere.2023.139087

Strand, S. M., Christiansen, H. H., Johansson, M., Åkerman, J., & Humlum, O. (2020). Active layer thickening and controls on interannual variability in the Nordic Arctic compared to the circum-Arctic. Permafrost and Periglacial Processes, 31(4), 575–592. https://doi.org/10.1002/ppp.2088

Stiegler, C., Johansson, M., Christensen, T. R., Mastepanov, M., & Lindroth, A. (2016). Tundra permafrost thaw causes significant shifts in energy partitioning. Tellus B: Chemical and Physical Meteorology, 68(1). https://doi.org/10.3402/tellusb.v68.30467

Tsai, Y.-L. S., Dietz, A., Oppelt, N., & Kuenzer, C. (2019). Remote Sensing of Snow Cover Using Spaceborne SAR: A Review. *Remote Sensing, 11*(12), 1456. https://doi.org/10.3390/rs11121456

Valman, S., Siewert, M. B., Boyd, D., Ledger, M., Gee, D., de la Barreda-Bautista, B., Sowter, A., & Sjögersten, S. (2024). InSAR-measured permafrost degradation of palsa peatlands in northern Sweden. The Cryosphere, 18(5), 1773–1790. https://doi.org/10.5194/tc-18-1773-2024

Westermann, S., Barboux, C., Bartsch, A., Delaloye, R., Grosse, G., Heim, B., Hugelius, G., Irrgang, A., Kääb, A. M., Matthes, H., Nitze, I., Pellet, C., Seifert, F. M., Strozzi, T., Wegmüller, U., Wieczorek, M., & Wiesmann, A. (2024a). *Permafrost Climate Change Initiative (Permafrost_cci): Product User Guide v4.1*. European Space Agency. https://dx.doi.org/10.5285/d34330ce3f604e368c06d76de1987ce5

Westermann, S., Barboux, C., Bartsch, A., Delaloye, R., Grosse, G., Heim, B., Hugelius, G., Irrgang, A., Kääb, A. M., Matthes, H., Nitze, I., Pellet, C., Seifert, F. M., Strozzi, T., Wegmüller, U., Wieczorek, M., & Wiesmann, A. (2024b). *Permafrost Climate Change Initiative (Permafrost_cci): Product Validation and Intercomparison Report v4.0. European Space Agency. https://climate.esa.int/en/projects/permafrost/*

Westermann, S., Barboux, C., Bartsch, A., Delaloye, R., Grosse, G., Heim, B., Hugelius, G., Irrgang, A., Kääb, A. M., Matthes, H., Nitze, I., Pellet, C., Seifert, F. M., Strozzi, T., Wegmüller, U., Wieczorek, M., & Wiesmann, A (2024c): ESA Permafrost Climate Change Initiative (Permafrost_cci): Permafrost active layer thickness for the Northern Hemisphere, v4.0. NERC EDS Centre for Environmental Data Analysis, 24 April 2024 https://climate.esa.int/en/projects/permafrost/

Westermann, S., Barboux, C., Bartsch, A., Delaloye, R., Grosse, G., Heim, B., Hugelius, G., Irrgang, A., Kääb, A. M., Matthes, H., Nitze, I., Pellet, C., Seifert, F. M., Strozzi, T., Wegmüller, U., Wieczorek, M., & Wiesmann, A. (2024d). *Permafrost Climate Change Initiative (Permafrost_cci): Algorithm Theoretical Basis Document (ATBD) v4.0*. European Space Agency. https://dx.doi.org/10.5285/d34330ce3f604e368c06d76de1987ce5

Xu, H., Chen, F., & Zhou, W. (2021). A comparative case study of MTInSAR approaches for deformation monitoring of the cultural landscape of the Shanhaiguan section of the Great Wall. *Heritage Science*, 9, 71. https://doi.org/10.1186/s40494-021-00543-y

Zebker, H. A., & Villasenor, J. (1992). Decorrelation in interferometric radar echoes. *IEEE Transactions on Geoscience and Remote Sensing*, 30(5), 950-959. https://doi.org/10.1109/36.175330

Appendix

Table S1: Results for 2018 measured ground truth active layer thickness compared to the InSAR based ALT estimations, as well as the absolute difference between the measured value and estimated value.

Site Name	Site Code	Measured (m)	InSAR Estimation (m)	Difference (m)
Heliport	AB5	0.90	1.01	0.11
Kursflaket	AB2	0.74	0.78	0.04
Mellanflaket	AB3	0.85	0.89	0.04
Storflaket	AB1	0.71	0.91	0.20
Torneträsk	AB4	1.46	1.01	0.45
Narkervare	AB11	1.01	1.06	0.05
Total Site	S2	0.95	0.94	0.01

Table S2: Results for 2019 measured ground truth active layer thickness compared to the InSAR based ALT estimations, as well as the absolute difference between the measured value and estimated value.

Site Name	Site Code	Measured (m)	InSAR Estimation (m)	Difference (m)
Heliport	AB5	0.91	0.82	0.09
Kursflaket	AB2	0.65	0.80	0.15
Mellanflaket	AB3	0.86	0.96	0.10
Storflaket	AB1	0.76	0.99	0.23
Torneträsk	AB4	1.50	1.11	0.39
Narkervare	AB11	0.96	1.06	0.10
Total Site	S2	0.94	0.96	0.02

Table S3: Results for 2020 measured ground truth active layer thickness compared to the InSAR based ALT estimations, as well as the absolute difference between the measured value and estimated value.

Site Name	Site Code	Measured (m)	InSAR Estimation (m)	Difference (m)
Heliport	AB5	0.99	0.67	0.32
Kursflaket	AB2	0.68	0.73	0.05
Mellanflaket	AB3	0.86	0.77	0.09
Storflaket	AB1	0.81	0.83	0.02
Torneträsk	AB4	1.50	1.37	0.13
Narkervare	AB11	0.95	1.36	0.41
Total Site	S2	0.97	0.96	0.01

Table S4: Results for 2021 measured ground truth active layer thickness compared to the InSAR based ALT estimations, as well as the absolute difference between the measured value and estimated value.

Site Name	Site Code	Measured (m)	InSAR Estimation (m)	Difference (m)
Heliport	AB5	0.97	1.06	0.09
Kursflaket	AB2	0.67	0.92	0.25
Mellanflaket	AB3	0.87	0.86	0.01
Storflaket	AB1	0.80	0.88	0.08
Torneträsk	AB4	1.50	0.89	0.61
Narkervare	AB11	1.09	1.05	0.04
Total Site	S2	0.98	0.94	0.04

Table S5: Results for 2022 measured ground truth active layer thickness compared to the InSAR based ALT estimations, as well as the absolute difference between the measured value and estimated value.

Site Name	Site Code	Measured (m)	InSAR Estimation (m)	Difference (m)
Heliport	AB5	1.10	0.81	0.29
Kursflaket	AB2	0.74	1.29	0.55
Mellanflaket	AB3	0.90	0.94	0.04
Storflaket	AB1	0.83	0.93	0.10
Torneträsk	AB4	-	-	-
Narkervare	AB11	1.15	0.77	0.38
Total Site	S2	0.94	0.95	0.01

Table S6: Results for 2023 measured ground truth active layer thickness compared to the InSAR based ALT estimations, as well as the absolute difference between the measured value and estimated value.

Site Name	Site Code	Measured (m)	InSAR Estimation (m)	Difference (m)
Heliport	AB5	1.06	1.28	0.22
Kursflaket	AB2	0.80	1.33	0.53
Mellanflaket	AB3	0.96	1.29	0.33
Storflaket	AB1	0.85	1.19	0.34
Torneträsk	AB4	-	-	-
Narkervare	AB11	1.20	1.37	0.17
Total Site	S2	0.97	1.29	0.32

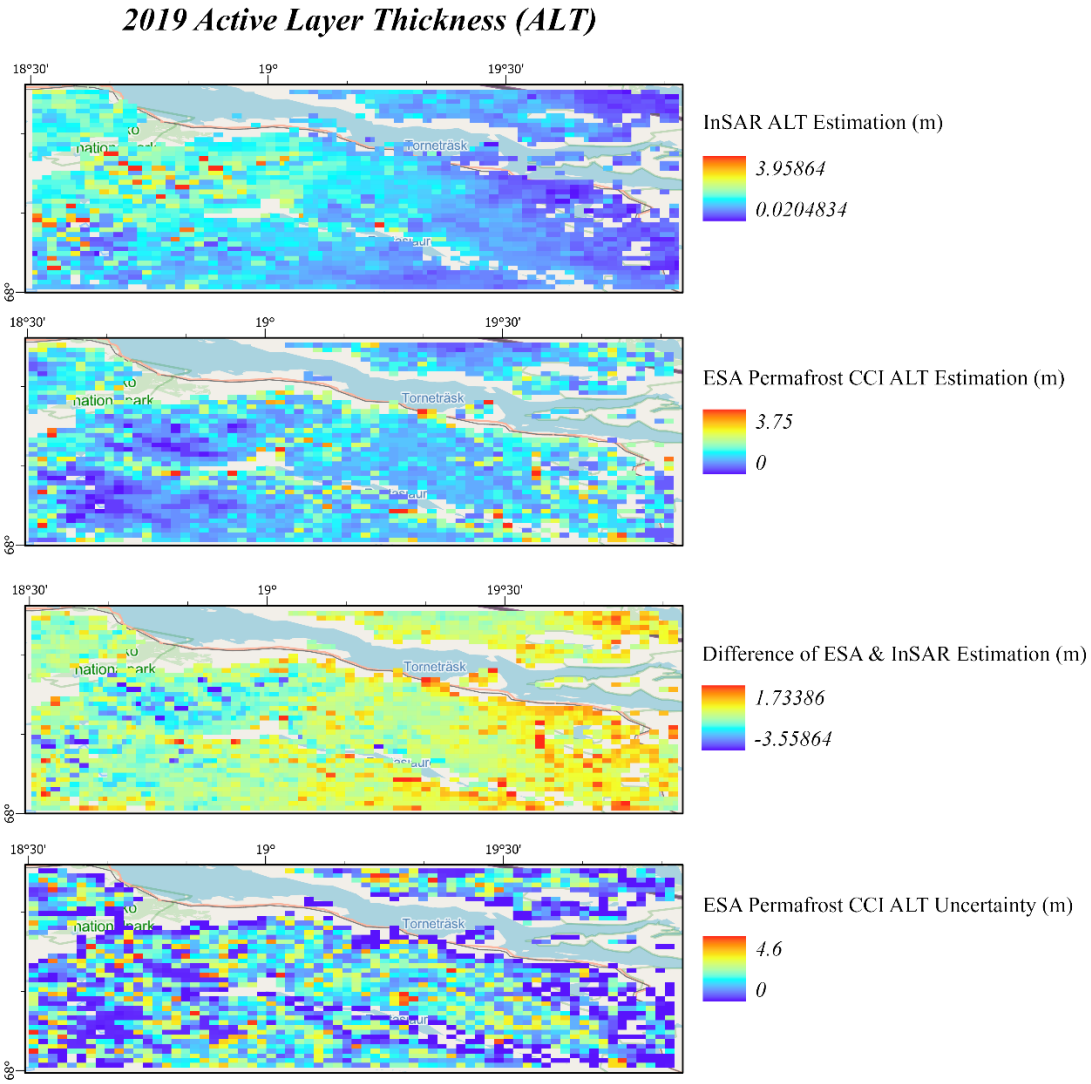

Figure S1: A four part data comparison of InSAR-based ALT, Permafrost_CCI ALT, the difference of the two (Permafrost_CCI – InSAR), and the CCI ALT uncertainty for 2019.

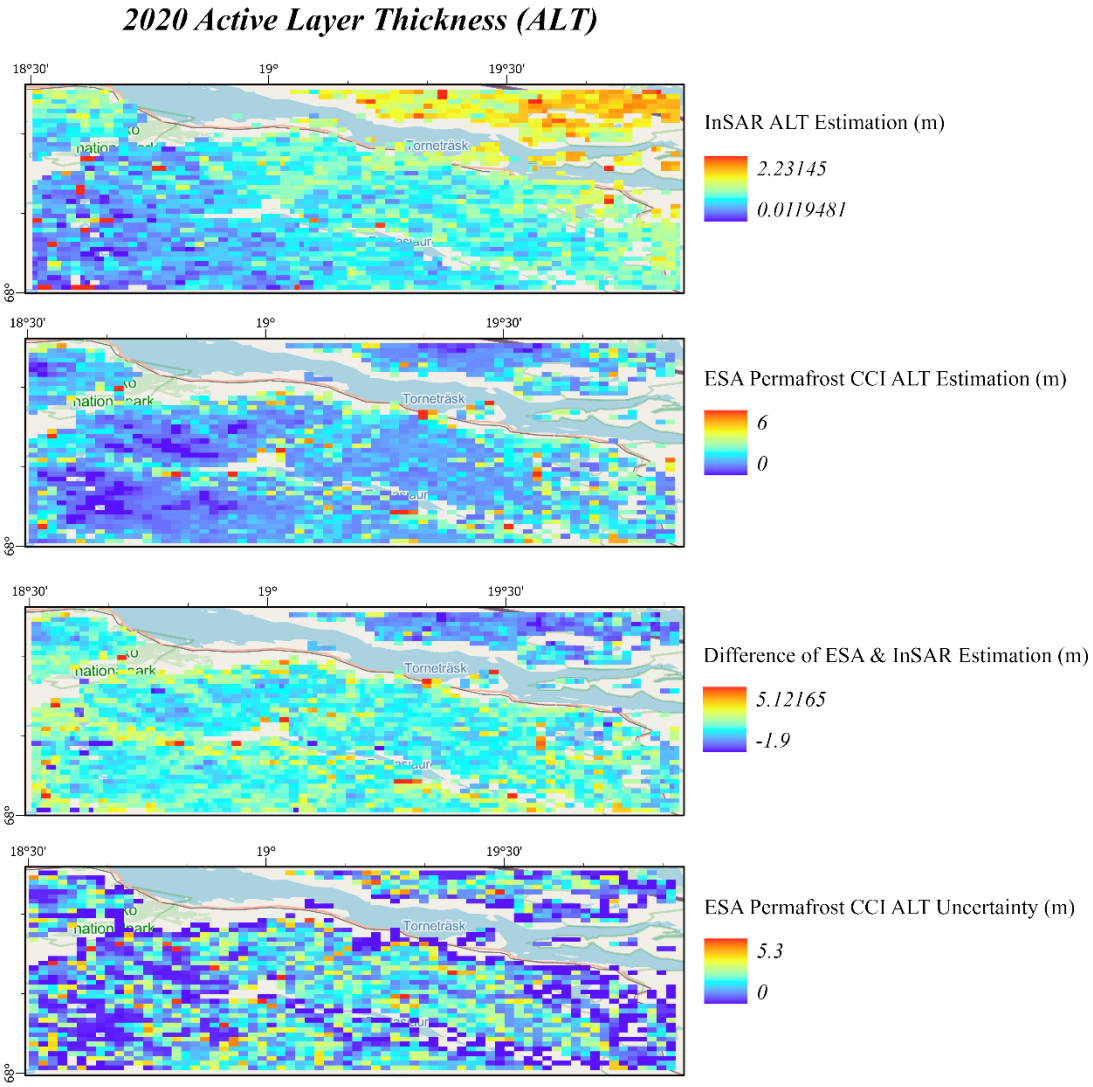

Figure S2: A four part data comparison of InSAR-based ALT, Permafrost_CCI ALT, the difference of the two (Permafrost_CCI – InSAR), and the CCI ALT uncertainty for 2020.

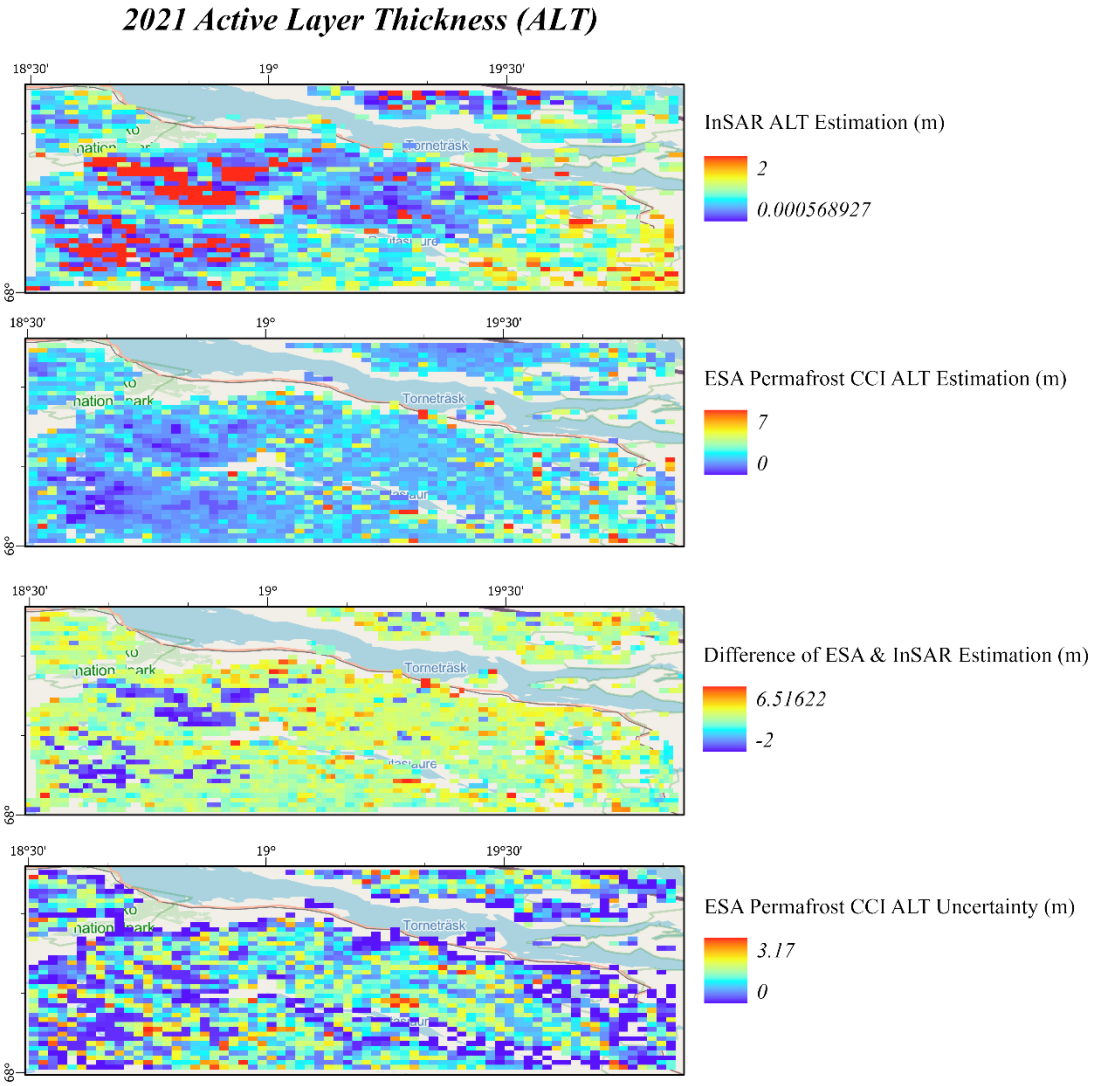

Figure S3: A four part data comparison of InSAR-based ALT, Permafrost_CCI ALT, the difference of the two (Permafrost_ CCI – InSAR), and the CCI ALT uncertainty for 2021.